Geol. Mag. **154** (*1*), *2017, pp. 147–165.* © *Cambridge University Press 2016*
doi:10.1017/S0016756815000941

Kinematic analysis of rock flow and deformation temperature of the Sirjan thrust sheet, Zagros Orogen, Iran

KHALIL SARKARINEJAD*, SAEEDE KESHAVARZ*†, ALI FAGHIH* & BABAK SAMANI‡

*Department of Earth Sciences, College of Sciences, Shiraz University, Shiraz, Iran
‡Faculty of Earth Sciences, Shahid Chamran University, Ahvaz, Iran

(*Received* 16 July 2015; *accepted* 23 October 2015; *first published online* 4 February 2016)

Abstract – Microstructural, finite strain and vorticity analyses of quartz-rich mylonites were used in order to investigate kinematics of rock flow and deformation temperature in the Sirjan thrust sheet exposed in a structural window within the Sanandaj–Sirjan High Pressure – Low Temperature (HP–LT) metamorphic belt that forms part of the hinterland of the Zagros orogenic belt of Iran. A dominant top-to-the-SW sense of shear in the study area is indicated by several shear sense indicators such as asymmetric boudins, rotated porphyroclasts, mica fish and S/C fabrics. Quantitative analyses reveal approximately plane strain deformation conditions with R_{xz} values ranging from 2.5 to 4.3 and increasing towards the Sirjan thrust. Opening angles of quartz c-axis fabrics and recrystallization regimes suggest deformation temperatures vary from 430 to 625 ± 50 °C in the hanging wall rocks. Oblique grain shape and quartz c-axis fabrics were used to estimate the degree of non-coaxiality during deformation. The obtained vorticity profile indicates a down-section increase in kinematic vorticity number (W_m) from 0.6 to 0.89. This range of vorticity numbers confirms contributions of both simple (41–68 %) and pure shear (32–59 %) deformation components. The structural characteristics of the study area ultimately were controlled by oblique motion of the Afro-Arabian plate relative to the Iranian plate.

Keywords: vorticity analysis, deformation temperature, finite strain, quartz fabrics, Zagros.

1. Introduction

Mid-crustal scale shear zones in the internal parts of mountain belts usually accommodate most of the regionally imposed deformation. Thus, kinematic reconstruction of rock flow within such shear zones is one of the most effective ways to constrain key aspects for the tectonic regime within orogenic systems. Use of vorticity analysis for estimating kinematics of rock flow in sheared rocks has proven to be a useful and effective tool for quantifying the nature and distribution of flow regimes within different tectonic settings including: contractional (Simpson & De Paor, 1997; Xypolias & Doutsos, 2000; Xypolias & Koukouvelas, 2001; Xypolias & Kokkalas, 2006), extensional (Wells, 2001; Bailey & Eyster, 2003; Faghih & Soleimani, 2015) and transpressional (Wallis, 1995; Klepeis, Daczko & Clarke, 1999; Holcombe & Little, 2001; Bailey, Francis & Fahrney, 2004) deformation regimes.

Microstructural studies on quartz are of great significance, especially for understanding the flow mechanisms and deformation patterns in natural shear zones (Bouchez & Pecher, 1981). Quartz c-axis fabric development is governed by the dominant slip systems and the strain path or the kinematic framework. Therefore, well-developed c-axis fabrics in mylonites can be used to characterize the kinematics of rock flow (Schmid & Casey, 1986; Sullivan & Law, 2007), the sense of shear (Law, 1990), the vorticity number associated with rock flow (Xypolias, 2009), the dominant deformation mechanisms (Lister & Dornsiepen, 1982; Stipp *et al.* 2002*a*) and the deformation temperature (Kruhl, 1996, 1998; Law, Searle & Simpson, 2004; Morgan & Law, 2004; Law, 2014). Variation in the degree of asymmetry of the quartz c-axis fabrics has also been used in many studies (Law, Knipe & Dayan, 1984; Law, Casey & Knipe, 1986; Platt & Behrmann, 1986; Ratschbacher, Wenk & Sintubin, 1991; Grujic *et al.* 1996; Xypolias *et al.* 2010; Wagner *et al.* 2010; Law *et al.* 2013) to infer vorticity gradients associated with emplacement of metamorphic rocks along ductile thrusts.

Many investigations have focused on the kinematics of rock flow within the Sanandaj–Sirjan High Pressure – Low Temperature (HP–LT) metamorphic belt (Mohajjel & Fergusson, 2000; Sarkarinejad, 2007; Sheikholeslami *et al.* 2008; Sarkarinejad, Faghih & Grasemann, 2008; Sarkarinejad, Godin & Faghih, 2009; Alizadeh, López-Martínez & Sarkarinejad, 2010; Sarkarinejad & Keshavarz, 2015), but few studies have been devoted to systematic study of the kinematics of flow in the high-grade metamorphic massifs. In this study, new microtectonic, finite strain, kinematic and vorticity data from ductile shear zones located in the Sirjan thrust sheet composed of high-grade metamorphic rocks within the HP–LT Sanandaj–Sirjan metamorphic belt are presented. The present study aims

†Author for correspondence: s.keshavarz2007@yahoo.com

to semi-quantify the ductile deformation conditions in this thrust sheet using quartz c-axis fabric data in order to obtain information on strain variations, deformation temperature and variations in kinematics at different structural positions based on detailed field observations and quantitative microstructural analyses. The main importance of this work lies in the fact that it provides a systematic study of the development of quartz c-axis fabrics in the Sirjan thrust sheet, which formed during progressive exhumation/ductile extrusion of gneissic basement rocks now exposed in a structural window, located in the eastern part of the Zagros Mountains.

2. Geological setting

The Zagros orogenic belt is a curvilinear part of the Alpine–Himalaya mountain range and forms the northeastern margin of the Afro-Arabian continent (Ricou, 1971; Alavi, 1994; Sarkarinejad, Partabian & Faghih, 2013). This belt is the result of Early to Middle Eocene closure of the Neo-Tethys by oceanic crust consumption on a NE-dipping subduction zone below the Iranian microcontinent, before Late Cretaceous to Tertiary continental collision between the Afro-Arabian continent and the Iranian microcontinent (Stöcklin, 1968; Dewey *et al.* 1973; Berberian & King, 1981; Blanc *et al.* 2003; Ghasemi & Talbot, 2006). The Zagros orogenic belt is composed of seven major subparallel tectonic elements (Sarkarinejad & Ghanbarian, 2014). They are, from southwest to northeast: (1) the Zagros foreland folded belt, (2) the Zagros foreland fold-and-thrust belt (Stöcklin, 1968; Berberian & King, 1981; Alavi, 1994), (3) the Zagros thrust system (ZTS; Sarkarinejad & Azizi, 2008), (4) the Zagros suture zone (Stöcklin, 1974; Sarkarinejad, 2005), (5) the Zagros hinterland fold-and-thrust belt (Sarkarinejad & Ghanbarian, 2014), (6) the Sanandaj–Sirjan HP–LT/HT–LP paired metamorphic belts (Sarkarinejad, 1999), and (7) the Urumieh–Dokhtar magmatic belt (Stöcklin, 1968) (Fig. 1). Subduction of the Neo-Tethyan oceanic crust was accompanied by widespread Mesozoic and syn- to post-Eocene calc-alkaline magmatism in the upper plate, along the Sanandaj–Sirjan HP–LT metamorphic belt and the Urumieh–Dokhtar magmatic arc, respectively (Agard *et al.* 2005). Post-collisional crustal shortening is still ongoing (Jackson & McKenzie, 1984; Allen, Jackson & Walker, 2004; Regard *et al*. 2004; Tatar, Hatzfeld & Ghafory-Ashtiyani, 2004) with a N–S-oriented convergence rate of approximately 20 ± 2 mm yr^{-1} in the direction N $8^{o} \pm 5^{\circ}$ E at the longitude of Bahrain (Vernant *et al*. 2004). Shortening in the basement occurs dominantly by faulting and folding. Mid-crustal rocks are exhumed or extruded at the surface as a result of thrusting or mid-crustal flow (Sarkarinejad, Godin & Faghih, 2009).

The Sanandaj–Sirjan HP–LT metamorphic belt is one of the major tectonic units of the Zagros orogen, which extends 1500 km along strike from the Bitlis area in Turkey to the western end of Makran and is 100 km wide (Sengör *et al.* 1988; McCall & Kidd, 1981; Mohajjel, Fergusson & Sahandi, 2003; Sarkarinejad, 2007). The Sanandaj–Sirjan HP–LT metamorphic belt is a coherent assemblage of tectonometamorphic units belonging to the upper Iranian plate (Mouthereau *et al.* 2007). This belt is part of a thrust system that has transported numerous slices of variously metamorphosed stratigraphic units from the northeast to southwest (Sarkarinejad & Azizi, 2008).

The study area is a structural basement window into the metamorphic complex in the Sanandaj–Sirjan HP–LT metamorphic belt (Fig. 1). It is located in the Sirjan, 25 km south of Sirjan city in the southeastern part of Iran. This basement window is situated between two ophiolite zones – Khoy-Neyriz and Naien-Baft (Ghasemi & Talbot, 2006) – and formed in the Zagros hinterland following collision of the Afro-Arabian continent and the Iranian microcontinent. The most predominant rocks in the study area consist of phyllite, micaschists, greenschists, quartzites, marble and crystalline dolomitic limestone (Fig. 2). In addition, sheared quartzo-feldspathic gneisses are exposed in the study area. The deformation and kinematic history recorded in the metamorphosed and deformed rocks of the Sirjan area is related to an inclined transpressional tectonic regime (Sarkarinejad, Partabian & Faghih, 2013).

3. Sirjan gneissic shear zones

The Sirjan basement window is a NNE-trending exposure of foliated gneissic rocks that are up to several hundred metres thick and located above the Sirjan thrust sheet associated with the Zagros thrust system (Sarkarinejad & Azizi, 2008). Metamorphic grade decreases from top to bottom so that the Sirjan thrust separates the gneissic rocks in the hanging wall from lower-grade metamorphic rocks in the footwall (Fig. 3a). The footwall block is mainly composed of metamorphic rocks such as greenschist, calc-schist, slate, phyllite, graphite schist and quartzite (Fig. 2). Marble can also be traced along contacts with other rocks and may be produced by thermal metamorphism. Footwall rocks have pervasive S/C fabrics, asymmetric boudins and folds that can be used to determine sense of shear (Fig. 3b).

Strongly sheared gneissic rocks in the hanging wall display fabrics ranging from proto- to-ultra mylonite. The main mineral assemblage is quartz + feldspar + plagioclase + biotite + muscovite + amphibole. Characteristic metamorphic minerals include garnet, tourmaline, zircon and apatite. Penetrative foliation and lineation were formed by alignment of mica flakes, stretched quartz and feldspar in the gneissic rocks. K-feldspar porphyroclasts are suspended in a fine-grained matrix of the aligned recrystallized quartz. Samples of an augen gneiss/sheared mylonite contain lenticular/sub-rounded clasts of δ-type and σ-type with asymmetric tails on K-feldspar porphyroclasts, in which the elongated feldspar grains define the S-foliation, whereas in the porphyroclast tails, mica,

https://doi.org/10.1017/S0016756815000941 Published online by Cambridge University Press

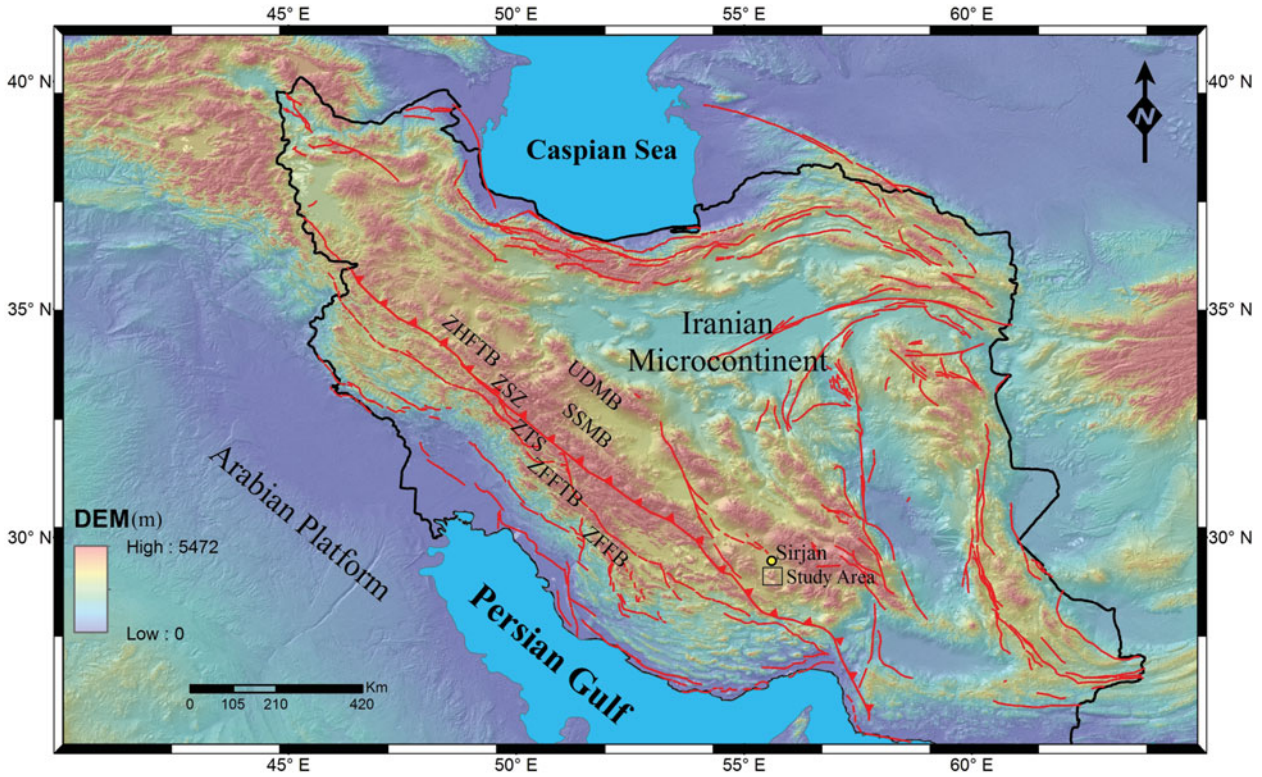

Figure 1. (Colour online) Shuttle Radar Topography Mission (SRTM) image depicting topographic relief of the structural domains of the Zagros orogen. Abbreviations: UDMB – Urumieh–Dokhtar Magmatic Belt; SSMB – Sanandaj–Sirjan Metamorphic Belt; ZHFTB – Zagros Hinterland Fold-and-Thrust Belt; ZSZ – Zagros Suture Zone; ZTS – Zagros Thrust System; ZFTB – Zagros Fold-and-Thrust Belt; ZFFB – Zagros Foreland Folded Belt.

amphibole and quartz form a C-foliation (Fig. 3c). In quartz-rich samples, mylonitic foliation is defined by shape-preferred orientation of elongate quartz ribbons (Fig. 4a). Small and sporadic leucogranite plutons intruded the middle part of the gneissic body. Fabrics in the small plutons have the same characteristics as in the country rocks, but their intensity is weaker.

4. Quartz microstructures

All microstructural and crystal fabric data are reported from oriented samples of quartz-rich gneisses. The samples were collected along a transect across the hanging wall to the Sirjan thrust. The fabric measurements were carried out on thin-sections cut perpendicular to foliation and parallel to stretching lineation. Observations on oriented thin-sections reveal that porphyroclasts in the mylonites are dominated by rigid and rotated K-feldspar and deformed biotite, while the matrix is made of recrystallized quartz, feldspar and biotite. Fine-grained quartz is deformed into tails that extend on both sides of the alkali-feldspar porphyroclasts, parallel to the mylonitic fabrics. These are σ-type and δ-type porphyroclasts (Passchier & Simpson, 1986). S/C fabrics also can be observed on the mesoscopic and microscopic scales. These structures are used as shear sense indicators. In the quartz-rich samples, elongate dynamically recrystallized quartz ribbons show a preferred alignment (SB) oblique to the macroscopic foliation (Fig. 4a). In all thin-sections the sense of obliquity indicates a top to- the-SW sense of shear.

Microstructures in the quartz grains (Fig. 4b, c) suggest development of grain-boundary migration (GBM) and sub-grain rotation (SGR) with minor microstructural evidence for bulging grain boundaries (BLG; Fig. 4c, d), which indicate dynamic recrystallization under Regime 2–3 conditions as defined by Hirth & Tullis (1992). Quartz crystallographic preferred orientation (CPO) is commonly observed in rocks that are dynamically recrystallized (Schmid & Casey, 1986). In general, the presence of a CPO is interpreted as evidence for significant deformation in the field of dislocation glide and creep (Vernooij, Brok & Kunze, 2006).

Quartz c-axis fabrics were measured on recrystallized quartz grains using an optical microscope and Leitz 5-axis universal stage, with an average of 300 grains being measured in each oriented sample. The universal stage data for c-axis orientations were plotted with respect to the mesoscopic foliation on an equal-area, lower hemisphere stereographic projection, and contoured using SpheriState 3.2 software. The data are summarized in Figure 5. From the density distribution of quartz c-axes, the fabrics may be interpreted as transitional Type 1 to Type 2 (Lister, 1977) cross-girdle c-axis fabrics indicating approximate plane strain deformation (Law, 1990). Fabric skeletons were traced by connecting the crests and ridges of each fabric

https://doi.org/10.1017/S0016756815000941 Published online by Cambridge University Press

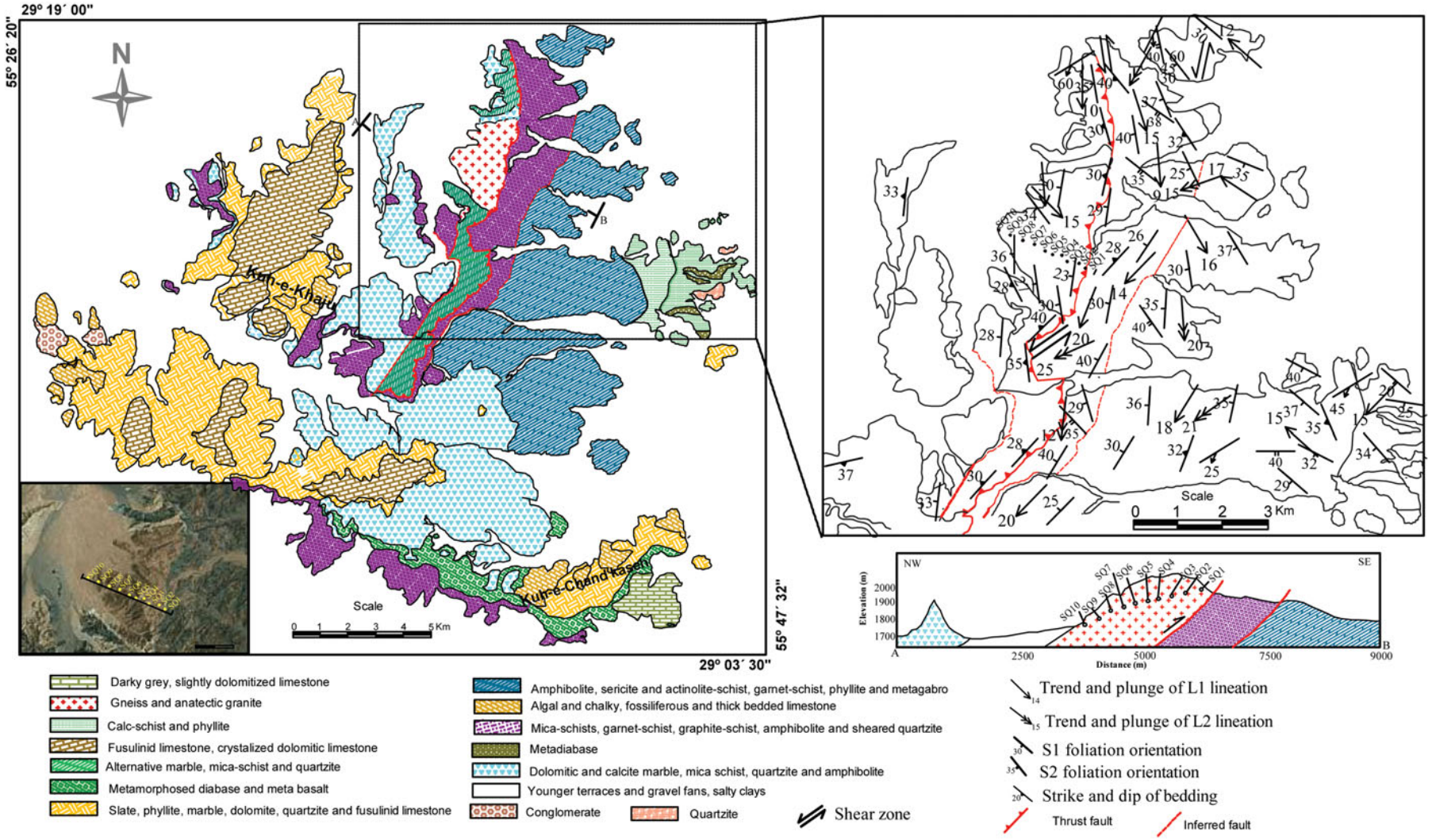

Figure 2. (Colour online) Geological map of the study area; spatial distribution of quartz c-axis samples is shown on the inset map through the transect line and detailed structural map of the study area showing the location of samples (filled circles) collected for strain symmetry, deformation temperature, vorticity and quartz petrofabric analyses.

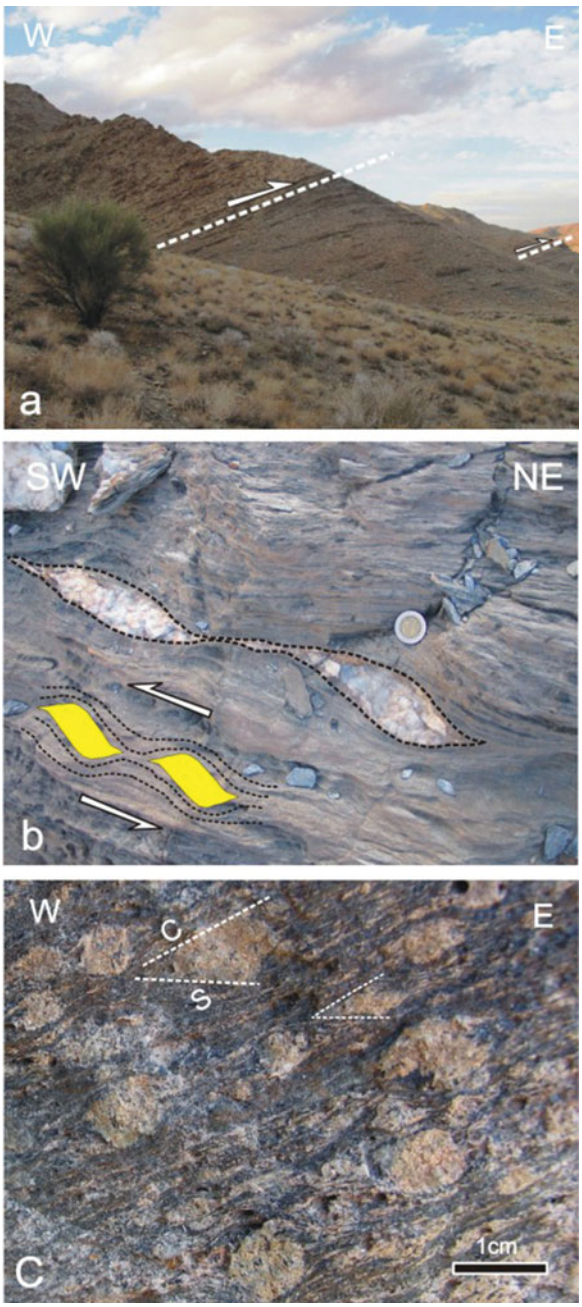

Figure 3. (Colour online) (a) View of the Sirjan thrust sheet which separates gneissic rocks in the hanging wall from the low-grade metamorphic rocks of the footwall. (b) Asymmetric shearband boudin train of a quartz vein in the schist host rock. (c) Quartzo-feldspathic mylonite with asymmetric tails of K-feldspar porphyroclasts and S/C fabrics indicates top-to-the-SW sense of shear.

diagram (Fig. 6; Lister & Williams, 1979; Lister & Hobbs, 1980). Skeletal analysis (Lister & Williams, 1979) of the contoured fabrics indicates an unequal inclination of the peripheral legs with respect to the central girdle segment (internal asymmetry) and an obliquity of the central girdle segment with respect to the foliation trace (external asymmetry). The sense of obliquity in all cases indicates a top-to-the-SW sense of shear (Fig. 6). Almost all c-axis fabrics exhibit monoclinic peripheral point-maxima asymmetry with respect to the main foliation, which is consistent with the c-axis pattern commonly reported for non-coaxial deformation (Wang *et al*. 2005). The obliquity of the central girdle segment (Ψ) varies between 71° and 82°.

External and internal fabric asymmetry may also be expressed by the relative magnitudes of the parameters C_1 and C_2 (external symmetry) and ω_1 and ω_2 (internal asymmetry) within individual samples (Platt & Behrmann, 1986; Law, 1987, 1990; Law *et al.* 2013). In our study samples, C_1 is smaller than C_2 indicating a top-to-the-SW sense of shear and ω_2 is consistently greater than ω_1, also consistent with non-coaxial deformation (Fig. 6; Table 1).

5. Shear sense indicators

Oriented thin-sections and hand samples were used to determine the spatial distribution of shear sense in deformed rocks from the study area. Thin-sections were cut parallel to lineation and perpendicular to foliation (XZ plane). Mica fish (Simpson & Schmid, 1983; Lister & Snoke, 1984; Passchier & Trouw, 2005) (Fig. 7a), δ- and σ-type asymmetric tails on porphyroclasts (Hanmer & Passchier, 1991; Passchier & Trouw, 2005; Fig. 7b, c), S/C shear plane (Figs 3c, 7d) and oblique quartz grain shape foliation (SB) in the Sirjan gneissic rocks (Fig. 4a) indicate a top-to-the-SW shear sense. The presence of cross-girdle quartz c-axis fabrics (Law, 1987) and their point maxima (Fig. 5) that are asymmetric with respect to the foliation and lineation also suggest a top-to-the-SW sense of shear.

On the mesoscopic scale, shear band boudins (Goscombe & Passchier, 2003; Goscombe, Passchier, & Hand, 2004; Pamplona & Rodrigues, 2011) in quartzite layers (Fig. 3b) and rotated porphyroclast and asymmetric folds (Hanmer & Passchier, 1991) confirm the top-to-the-SW sense of shear (Fig. 3c). All macroscopic and microscopic shear criteria support a non-coaxial flow regime.

6. Deformation thermometry

Three analytical methods were used to assess deformation temperatures recorded in the hanging wall of the Sirjan thrust sheet: (1) the stability fields of metamorphic mineral assemblages present within quartz-rich mylonite (cf. Jessell, 1987; Hirth & Tullis, 1992; Fitz Gerald & Stünitz, 1993; Lloyd & Freeman, 1994; Hirth, Teyssier & Dunlap, 2001; Stipp *et al.* 2002*a*, *b*), (2) the opening angle in the quartz c-axis lattice preferred orientations (Kruhl, 1998; Law, Searle & Simpson, 2004; Law, 2014), and (3) quartz slip systems inferred from quartz lattice preferred orientations (Mainprice *et al.* 1986; Tullis & Yund, 1992).

Quartz grains exhibit undulose extinction, deformation bands, weak shape-preferred orientation, locally strong crystal-preferred orientation, oblique foliation and locally developed core-and-mantle structures, indicating deformation temperatures of 400–600 °C

https://doi.org/10.1017/S0016756815000941 Published online by Cambridge University Press

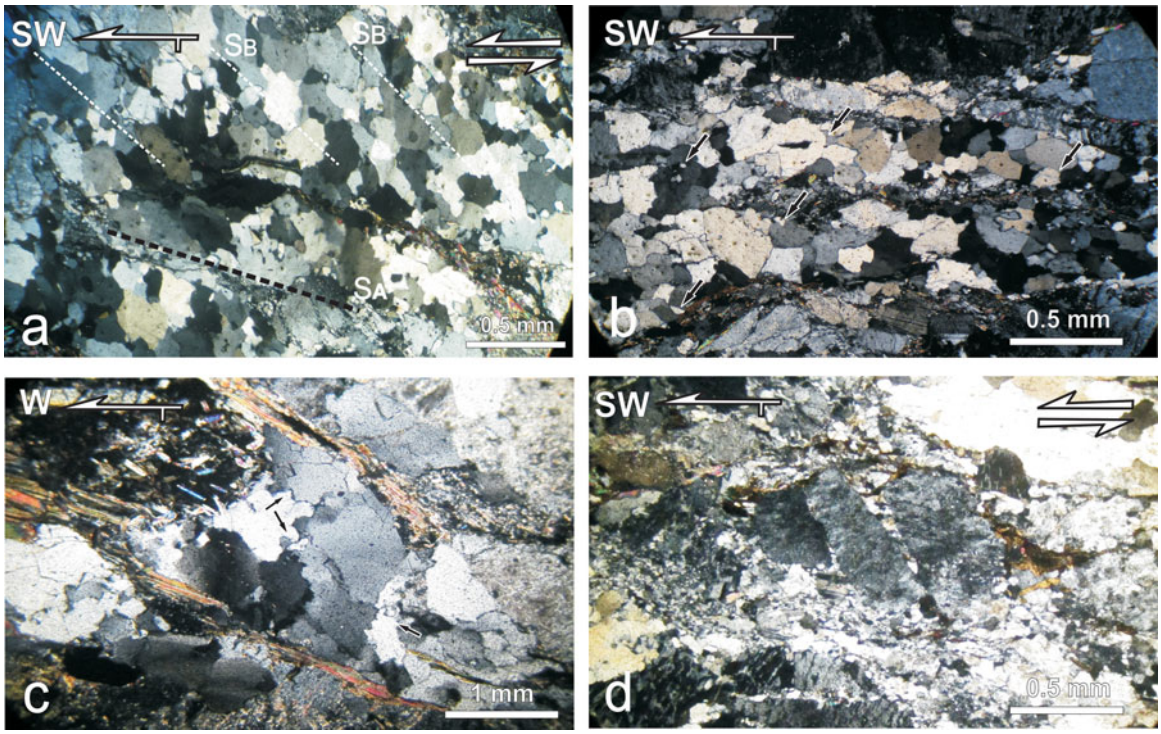

Figure 4. (Colour online) Photomicrographs of quartz fabrics. All sections cut perpendicular to foliation and parallel to stretching lineation (crossed polarized light). (a) Oblique grain shape in the dynamically recrystallized quartz grains. SA (black dashed line) denote the main foliation and SB (white dashed line) the oblique foliation. (b) Ribbon quartz; the slightly sutured shape of the high-angle grain boundaries suggest that sub-grain rotation (SGR) was active. (c) Quartz exhibiting bulging (BLG) recrystallization at quartz grain boundaries indicating deformation temperatures of 280–400 °C overprinting a higher temperature fabric. (d) Mylonite with domino-like structure of antithetic shear along micro-faults on the K-feldspar porphyroclasts. Grain-boundary migration recrystallization of quartz textures in matrix indicating deformation temperatures of 500–650 °C.

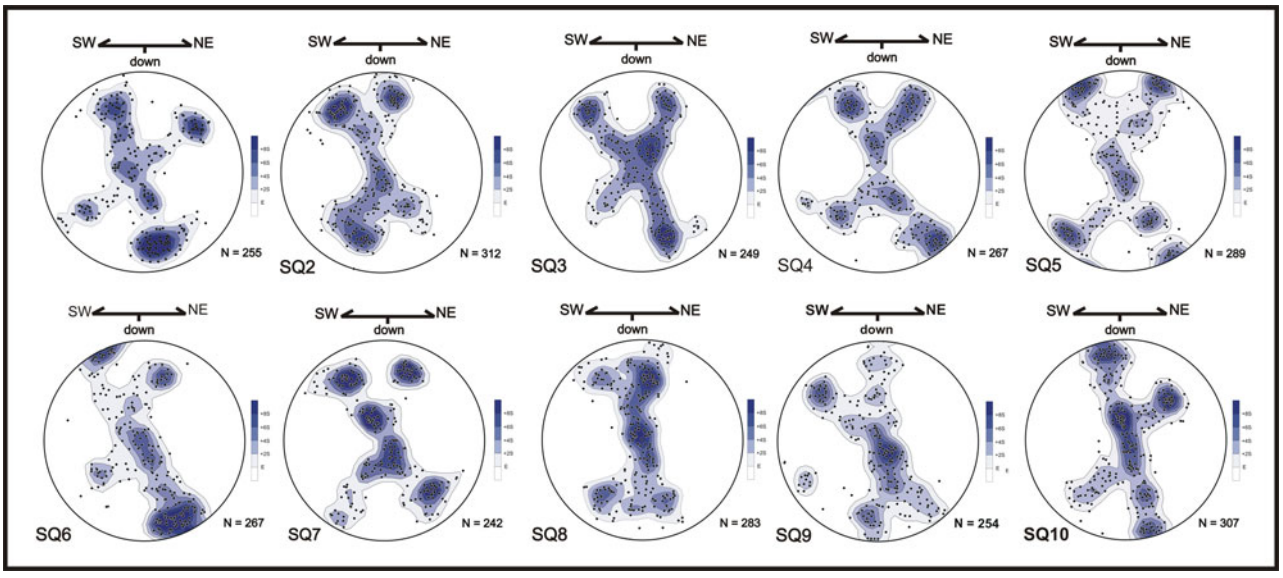

Figure 5. (Colour online) Optically measured quartz c-axis fabrics of selected quartz-rich samples: equal-area, lower hemisphere stereographic projections; foliation is orientated left–right and vertical; lineation is horizontal; contour intervals: 2, 4, 6 and 8 times uniform distribution. N – number of grains measured in each sample.

(Stipp *et al*. 2002*a*). Deformation temperature estimates can be obtained using quartz deformation microstructures preserved under different recrystallization conditions (Fig. 8a). Low temperature deformation (280–400 °C) is indicated by bulging microstructures (BLG), intermediate temperatures (400–500 °C) are suggested by sub-grain rotation recrystallization microstructures (SGR) and high temperatures (> 500 °C) can be inferred from grain-boundary migration recrystallization microstructures (GBM) (Stipp *et al*. 2002*a*,*b*). At temperatures > 650 °C quartz exhibits chessboard extinction (Lister & Dornsiepen, 1982).

https://doi.org/10.1017/S0016756815000941 Published online by Cambridge University Press

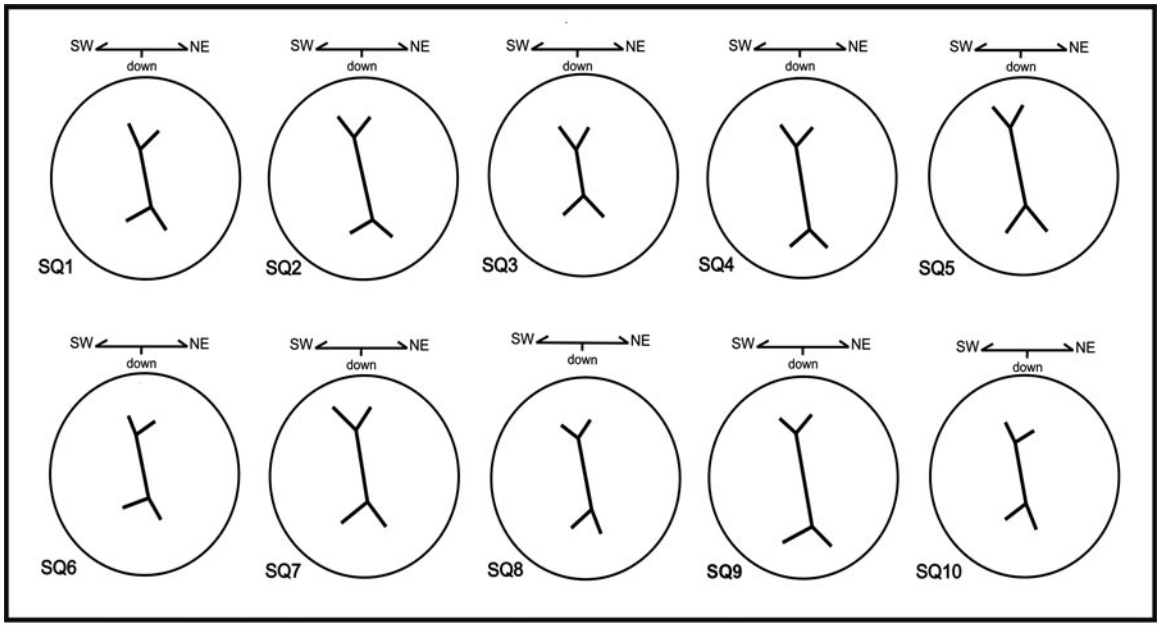

Figure 6. Quartz c-axis fabric skeletons of individual samples from the study area. The observed fabric asymmetry indicates a significant component of non-coaxial, top-to-the-SW or sinistral sense of shear. Sample location details given in Figure. 2.

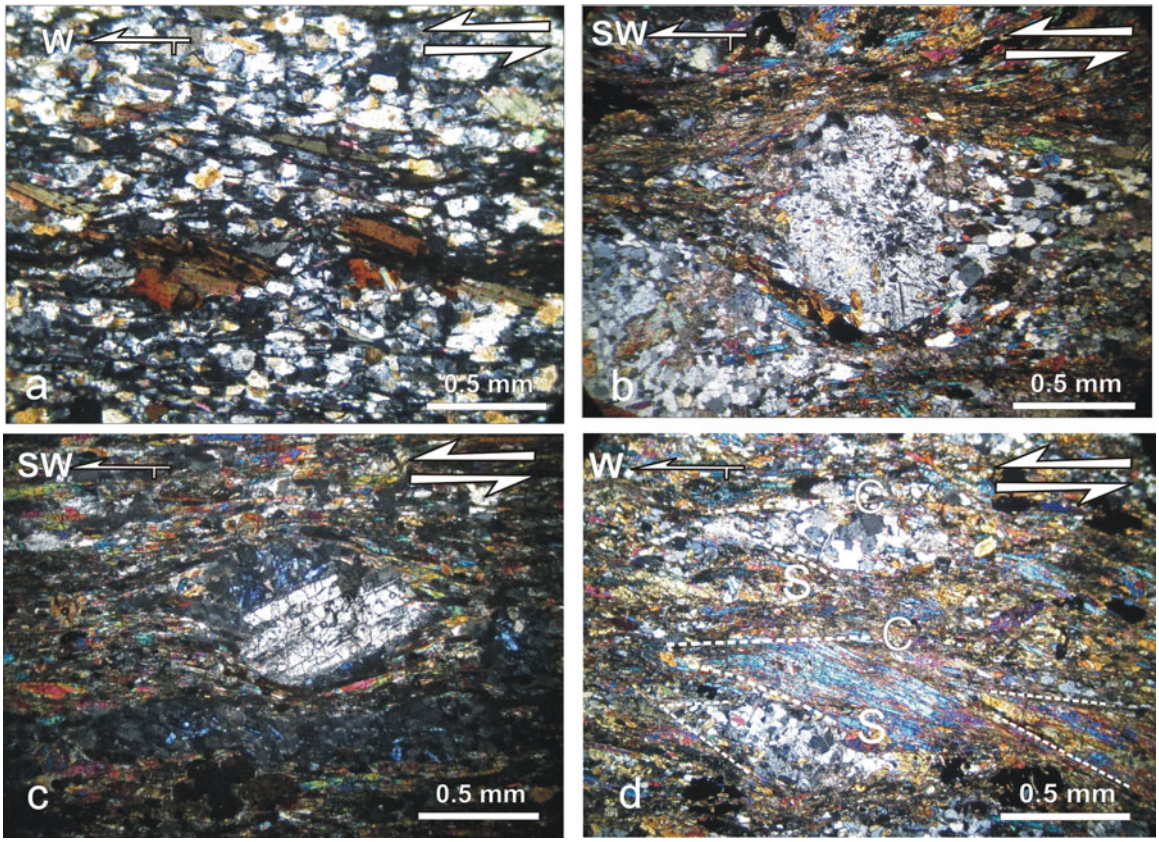

Figure 7. (Colour online) Photomicrographs of kinematic indicators from the Sirjan thrust sheet. All photomicrographs are perpendicular to the foliation and parallel to stretching lineation, which display a sinistral sense of shear. (a) Ultramylonite with mica fish indicating top-to-the-W sense of shear; crossed polarized light. (b) Photomicrograph of mylonite with δ-type alkali-feldspar porphyroclasts and recrystallization of the quartz and feldspar by bulging in the matrix, its asymmetry trail indicating top-to-the-W shear sense. (c) Photomicrograph of a σ-type K-feldspar porphyroclast with muscovite wings. (d) Photograph of S/C fabric, with S inclined to the right and C subhorizontal, which is well developed and indicates a sinistral sense of shear.

https://doi.org/10.1017/S0016756815000941 Published online by Cambridge University Press

Table 1. Details of quartz c-axis fabrics, strain and vorticity analysis for quartz-rich samples from the study area. Sample location details given in Figure 2

	Quartz c-axis fabric asymmetry Parameters						Finite strain	Vorticity analysis (W_m)	
Sample	C_1°	C_2°	ω_1°	ω_2°	β°	δ°	R_{xz}	Method I	Method II
SQ1	33	65	11	47	11–15	14	4.3	0.77–0.89	0.76–0.84
SQ2	51	61	24	43	11–14	13	4.0	0.75–0.85	0.78–0.80
SQ3	44	50	31	38	10–14	10	3.6	0.67–0.82	0.64–0.74
SQ4	43	54	27	52	10–13	–	3.9	0.70–0.81	–
SQ5	36	41	30	50	9–11	11	3.55	0.62–0.71	0.64–0.68
SQ6	34	68	11	68	8–11	10	3.35	0.60–0.73	0.60–0.66
SQ7	32	40	35	46	8–11	–	3.0	0.51–0.65	–
SQ8	36	71	37	45	9–13	–	2.8	0.52–0.69	–
SQ9	38	53	38	40	10–14	10	2.65	0.59–0.75	0.61–0.71
SQ10	51	56	17	70	11–13	9	2.5	0.60–0.68	0.64–0.69

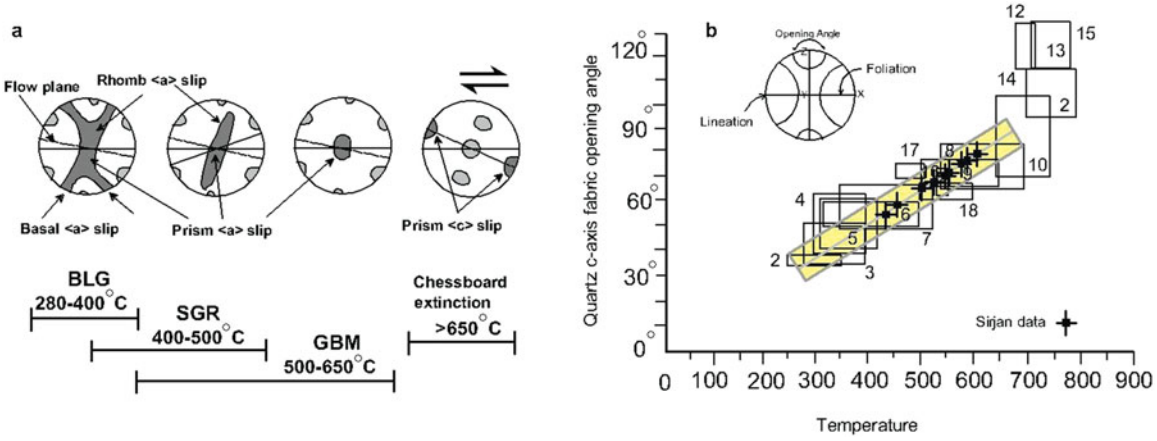

Figure 8. (Colour online) (a) Simplified stereonets showing the dependence of quartz LPOs and inferred slip systems on increasing temperature during non-coaxial deformation and plane strain (see text). Quartz c-axes are shown in dark grey and <a> axes in light grey. Modified from Passchier & Trouw (2005). (b) Relationship between c-axis opening angle to temperature. Grey line is the best-fit line with ± 50 °C error. X, Y and Z strain axes are shown. Boxes 1–15 from Kruhl (1998); boxes 16–18 indicate data from Law *et al.* (1992), Nyman, Law & Morgan (1995) and Okudaira *et al.* (1995), respectively; boxes 19 and 20 from Langille *et al.* (2010). Data from this study are shown. Modified from Law, Searle & Simpson (2004).

In the case of plane strain, the opening angle (OA) is defined as the angle between the two girdles of the c-axis cross-girdle lattice preferred orientations, measured in the plane perpendicular to foliation and parallel to lineation (Fig. 8a). A positive correlation exists between opening angle and deformation temperature from 250 °C to 650 °C, although hydrolytic weakening and changes in strain rate also play a role (Law, 2010). According to Kruhl (1998), modified by Law, Searle & Simpson (2004), the geothermometer correlates graphically with the opening angle of quartz c-axis fabrics with increasing deformation temperature, with an uncertainty of ± 50 °C (Fig. 8b). In our study, quartz c-axis fabric opening angles display a systematic variation with respect to structural distance from the underlying Sirjan thrust. Our samples have opening angles ranging from 56° to 80° (Fig. 6). These data provide a confirmation of the relationship between increasing opening angle and deformation temperature between ~ 430º and 625 °C (Fig. 8b).

Additionally, because quartz c-axis fabric pattern is also a function of temperature and strain rate, such fabrics indicate the activation of different slip systems during deformation. At low temperatures (lower-greenschist facies) and faster strain rates, basal <a> slips results in c-axis point maxima forming near the Z-axis of the finite strain ellipsoid (Bouchez, 1977; Bouchez & Peĉher, 1981; Schmid & Casey, 1986). With increasing temperature (mid-greenschist facies), rhomb <a> slip is activated, forcing the c-axis maxima to migrate to intermediate positions between the Y- and Z-axes. Under amphibolite-facies conditions the prism <a> slip system begins to be activated, resulting in point maxima near the Y-axis (Lister & Dornsiepen, 1982; Mainprice *et al.* 1986; Schmid & Casey, 1986). Ultimately, at temperatures higher than 700 °C, prism <c> slip is activated, with c-axes concentrating near the X-axis (Mainprice *et al.* 1986; Cavalcanti De Araújo *et al.* 2003) (Fig. 8a). In this study, quartz fabric diagrams indicate a progressively increasing contribution of prism <a> slip, relative to basal <a> and rhomb <a> slip, with increasing distance from the underlying Sirjan thrust (Fig. 5). These thermometers yield information on deformation temperatures for the time during thrusting/exhumation at which ductile deformation, such as dislocation and dynamic recrystallization, stopped and crystallographic fabrics were locked in for individual samples (cf. Law *et al.* 2013).

https://doi.org/10.1017/S0016756815000941 Published online by Cambridge University Press

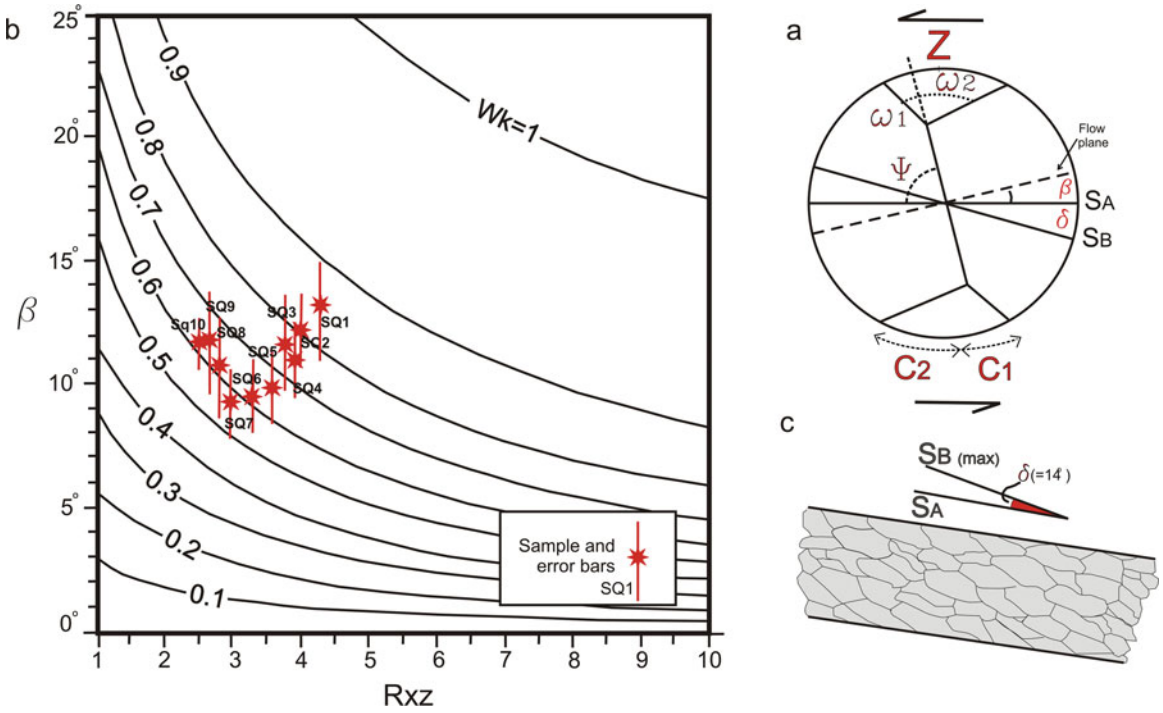

Figure 9. (Colour online) (a) Fabric skeleton and angular relationships between quartz c-axis and external and internal fabric asymmetry. (b) Plot of β versus R_{xz} (principal normal strain ratio in the XZ plane) contoured for different W_k (Tikoff & Fossen 1995; Grasemann, Fritz & Vannay, 1999). Length of error bars reflects degree of uncertainty in measuring β in each sample; stars indicate β value (Table 1) obtained from 'best-fit' skeleton. The majority of the measured ten samples indicate W_k between 0.51 and 0.89. (c) Alignment (SB) of elongate dynamically recrystallized quartz grains orientated oblique to macroscopic foliation (SA); δ angle defined as a maximum angle between grain long axes and foliation. Both diagrams (b) and (c) are drawn in the XZ plane and indicate a sinistral shear sense.

7. Kinematic vorticity analysis

Vorticity analysis enables estimation of the relative contributions of pure and simple shear components during ductile deformation. For plane strain deformation, components of pure shear and simple shear can be quantified in terms of the kinematic vorticity number W_k (Means, 1994) that ranges between 1.0 if deformation occurs under simple shear condition and 0 for pure shear. Sub-simple shear is the term used for flows between pure and simple shear ($1>W_k>0$) (Passchier & Trouw, 2005). Equal contributions of pure and simple shear occur at $W_k = 0.71$ (Law, Searle & Simpson, 2004). In natural systems the vorticity of flow may vary with both space and time. In such cases of non-steady-state deformation, flow may be more appropriately characterized by the mean kinematic vorticity number W_m, in which the vorticity of flow is integrated over space and time (Passchier, 1988). For steady-state deformation W_k (instantaneous deformation) $= W_m$ (finite deformation; Passchier, 1988).

In the past two decades a number of vorticity gauges have been suggested for quantifying the degree of non-coaxiality of flow in deformed rocks (e.g. Passchier, 1987, 1988; Wallis, 1992, 1995; Wallis, Platt, & Knott, 1993; Simpson & De Paor, 1997; Holcombe & Little, 2001; Law, Searle & Simpson, 2004; Jessup, Law & Frassi, 2007; Gomez-Rivas *et al.* 2007; Sullivan, 2008). Recent vorticity studies indicate that differences in W_m from sample to sample can be detected with the use of the quartz c-axis fabric and strain ratio method (Wallis, 1992, 1995; Grasemann, Fritz & Vannay, 1999; Law, Searle & Simpson, 2004; Xypolias, 2009).

Our samples from quartz-rich layers within the gneisses above the Sirjan thrust are appropriate for two methods of vorticity measurements: (1) the strain ratio / quartz c-axis fabric method (R_{xz}/β-method), and (2) the oblique recrystallized grain / quartz c-axis fabric method (δ/β-method). These two methods were employed on data collected from thin-sections cut parallel to lineation and perpendicular to foliation. Both methods assume a vorticity vector oriented perpendicular to the maximum and minimum principal axes of finite strain (i.e. it lies along the intermediate principal stretching rate axis during progressive flow) (Tikoff & Fossen, 1995) and the presence of a steady-state non-coaxial flow that leads to formation of monoclinic or orthorhombic symmetry (Lin, Jiang & Williams, 1998; Passchier, 1998).

7.a. Method I: strain ratio / quartz c-axis fabric (R_{xz}/β-method)

In the study area quartz-rich samples are characterized by Type 1 crossed-girdle quartz c-axis fabrics which exhibit an asymmetry with respect to the trace of foliation in the XZ plane. The angle β between the perpendicular to the central girdle of the quartz c-axis fabric skeleton and main foliation is equal to the angle between the flow plane and principal plane of strain (Fig. 9a). The angle

https://doi.org/10.1017/S0016756815000941 Published online by Cambridge University Press

β is a function of R_{xz} (strain ratio) and is expressed by Xypolias (2009) as:

$$W_m = \cos\left[\tan^{-1}\left(\frac{R_{xz}\tan^2\beta}{(1+R_{xz})\tan\beta}\right)\right]$$

Alternatively, estimates of W_m can be obtained graphically using the diagram shown in Figure 9b, which summarizes relationships between R_{xz} and β for various W_m values. Note that the R_{xz}/β-method is equivalent to the R_{xz}/θ′-method (Tikoff & Fossen, 1995; Bailey & Eyster, 2003), which uses the angle (θ′) between the long axis of the finite strain ellipsoid and the shear zone boundary to estimate W_m.

The finite strain ratio in the XZ plane (R_{xz}) was estimated using the R_f/Φ-method (Ramsay & Huber, 1983; Lisle, 1985) on elliptical strain markers such as plastically deformed quartz grains in quartz-rich samples. For each thin-section, at least 80 deformed quartz grains were measured. Note that these R_{xz} values were calculated from the shape of plastically deformed elongate, slightly recrystallized quartz grains lying in the plane of the main foliation while analyses of shape data were performed using algebraic and geometric R_f/Φ methods (e.g. Xypolias, Chatzaras & Koukouvelas, 2007; Xypolias, 2009; Samani, 2013). R_f/Φ diagrams were constructed using the software of Chew (2003). Calculated strain ratios in the XZ plane range between 2.5 and 4.3 (Fig. 10; Table 1).

The Wallis (1995) method of vorticity analysis has been widely used in studies of natural shear zones (e.g. Xypolias & Doutsos, 2000; Law, Searle & Simpson, 2004; Sullivan, 2008; Law, 2010; Sarkarinejad, Partabian & Faghih, 2013; Xypolias *et al.* 2010). The key assumption of this method is that the central girdle of quartz c-axis fabrics develops orthogonal to the flow/shear plane during general shearing. This assumption is strongly supported by both experimental (e.g. Bouchez & Duval, 1982; Herwegh & Handy, 1996; Herwegh, Handy & Heilbronner, 1997) and numerical simulation of quartz crystal fabric formation (e.g. Lister & Hobbs, 1980; Etchecopar & Vasseur, 1987), as well as by observations in natural quartz mylonites (e.g. Burg, 1986; Law, 1990; Sullivan & Law, 2007). Uncertainty in determination of the β angle is by far the largest source of error in W_m estimates obtained by this method (e.g. Grasemann, Fritz & Vannay, 1999; Law *et al.* 2010). Therefore, the method was applied to ten samples where the β angle could be determined with an uncertainty smaller than ± 3°. Error bars estimated by the maximum and minimum β-values for each sample are shown in the R_{xz}/β diagrams of Figure 9b. Note also that for the analysed samples, the error in W_m values arising as a consequence of the uncertainty in estimating strain ratio is always overlapped by the error in W_m produced by the uncertainty in assigning β values (Xypolias *et al.* 2010). Analysis of our samples yielded W_m values ranging from 0.51 to 0.89 (Table 1).

7.b. Method II: oblique grain shape/quartz c-axis fabric method (δ/β-method)

This method was originally proposed by Wallis (1995) and is based on the assumption that newly formed recrystallized quartz grains within an oblique grain shape fabric (SB) initially grow with their long axes nearly parallel to the extensional instantaneous stretching axis (ISA_1) of flow. The acute angle (η) is defined as the angle between the line of zero instantaneous rotation or flow apophysis (A_i) and instantaneous stretching axes (ISA; Passchier, 1988). For steady-state deformation, the orientation of the ISA_1 is related to W_m by the following equation (Wallis, 1995):

$$W_m = \sin 2\eta = \sin = 2(\delta + \beta)$$

where β is the angle between foliation and the flow plane, which is inferred to be perpendicular to the central segment of the cross-girdle fabric, and the δ angle is inferred to be the maximum inclination angle between the long axis of elongate oblique dynamically recrystallized quartz grains (SB) and the main foliation (SA) (Fig. 9c).

This method has proved applicable to seven samples that are characterized by both an oblique grain shape (SB) and cross-girdle quartz c-axis fabrics. Within individual samples, determination of the δ angle was based on at least 90 orientation measurements of the long axes of oblique recrystallized grains with respect to the main foliation (SA). The angle δ was assigned to be the maximum angle from each continuous population of readings (Frassi *et al*. 2009; Xypolias *et al.* 2010). This analytical method yielded W_m estimates ranging from 0.6 to 0.84 (Table 1).

W_m estimates using the δ/β-method are not sensitive to small uncertainties in β-values. Although uncertainties in assigning δ have not been investigated so far, their effect on W_m estimates is not expected to be great (Xypolias, 2010). Uncertainties in vorticity values estimated by applying this technique can be attributed to (1) heterogeneity of matrix material, (2) the presence of porphyroclasts, and (3) folding, which may deflect or influence the orientation of the quartz fabric (Langille *et al.* 2010). To limit possible inaccuracies, measurements were made from quartz fabrics that were unaffected by these potential problems.

8. Discussion

8.a. Deformation temperatures and apparent thermal gradient within the mylonitic Sirjan thrust sheet

Quartz lattice preferred orientations and microstructures reflect deformation conditions and can be used for the estimation of deformation temperatures. The quartzo-feldspathic mylonites from the study area have opening angles ranging from 56° to 80°. Using the Kruhl (1998) thermometer these opening angles indicate deformation temperatures ranging from 430 to 625 °C traced from the SE to NW along our sampling transect. The opening angles of the quartz fabric

https://doi.org/10.1017/S0016756815000941 Published online by Cambridge University Press

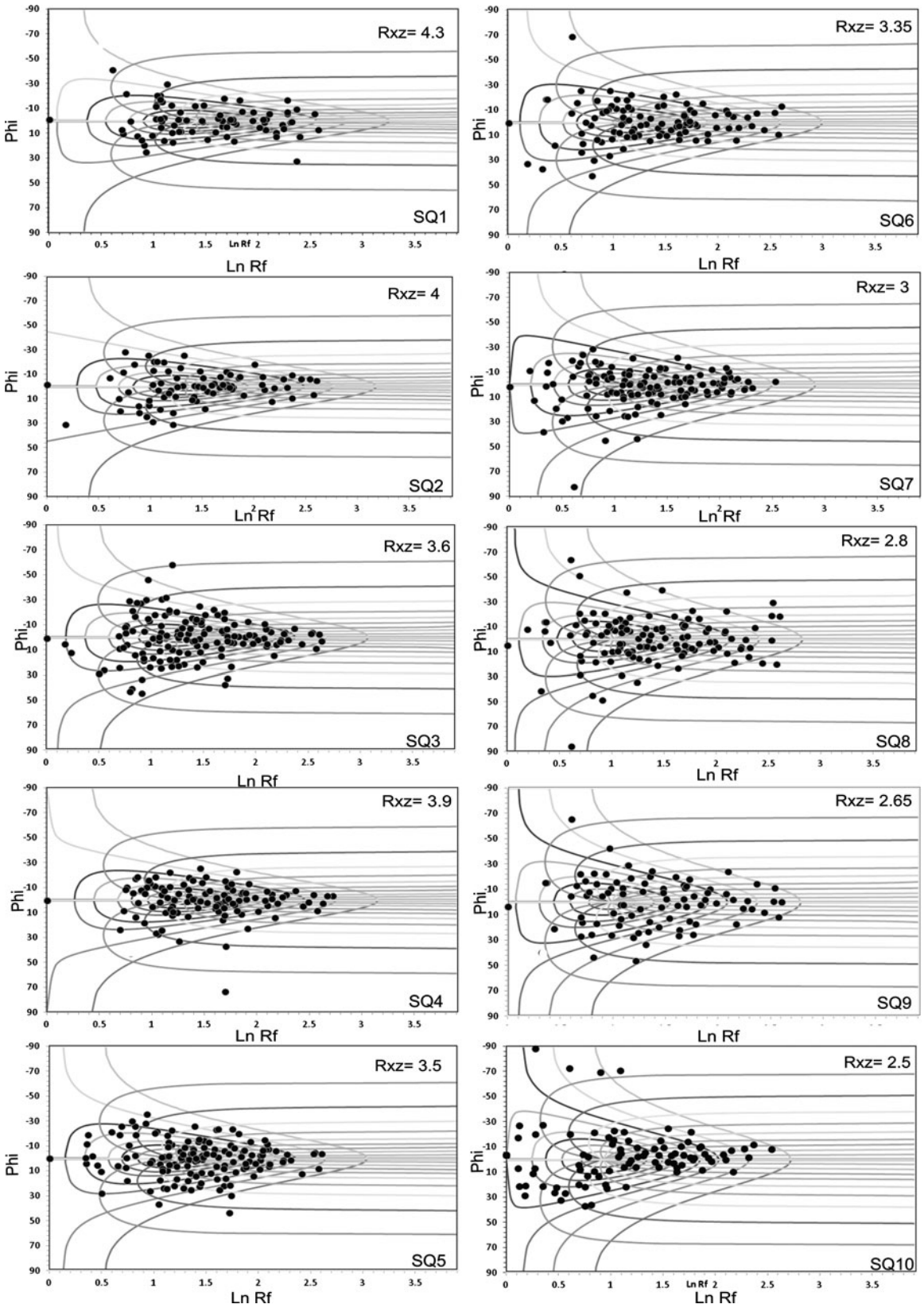

Figure 10. Estimation of R_{xz} finite strain parameters from the Rf/Φ method for the same collection of specimens.

skeletons and inferred deformation temperatures are plotted against the structural distance above the Sirjan thrust in Figure 11. A linear regression line through these data indicates an apparent thermal field gradient of 253 °C per km. A power law fit indicates a steeper apparent thermal gradient (~ 229 °C per km) at less than 600 m above the Sirjan thrust, which decreases to 89 °C per km at 600–900 m. The smooth upward increase in quartz c-axis opening angles and inferred deformation temperatures traced from the SE to NW,

https://doi.org/10.1017/S0016756815000941 Published online by Cambridge University Press

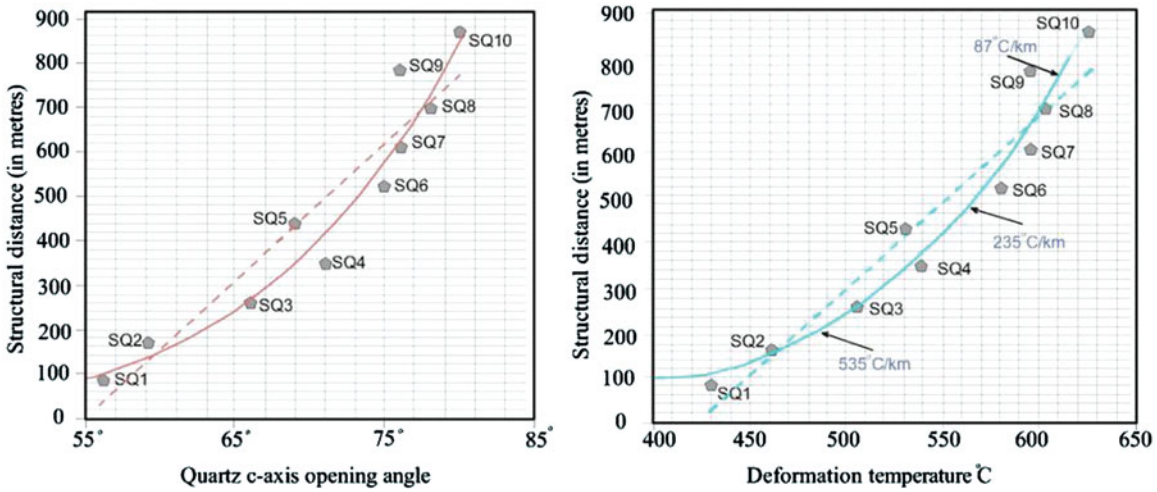

Figure 11. (Colour online) Quartz c-axis opening angles and inferred deformation temperatures plotted versus structural distance above the Sirjan thrust for samples collected along the NW–SE transect line shown in Figure 2. Deformation temperatures estimated by using the Kruhl (1998) fabric opening-angle thermometer have a nominal ± 50 °C uncertainty. Power law best-fit curves and linear regression best-fit lines indicated by solid and dashed lines, respectively. Apparent thermal field gradients between samples also indicated. Sample location details given in Figure. 2.

together with the steadily decreasing thermal field gradient (Fig. 11), suggest that shearing was pervasively distributed at the grain scale, rather than being concentrated on isolated individual shear surfaces (Jain & Manickavasagam, 1993, 1997; Hubbard, 1996, 1997) with shearing progressively decreasing in magnitude with distance above the Sirjan thrust.

The distribution of deformation temperatures based on quartz opening angles is in good agreement with deformation temperatures indicated by quartz recrystallization microstructures. Samples which exhibit dominantly rhomb <a> and prism <a> slip along with minor basal <a> slip based on the topology of the quartz c-axis fabrics (Fig. 5) display quartz microstructures suggesting sub-grain rotation recrystallization and opening angles indicating deformation temperatures of 400–500 °C. In contrast, the limited evidence for grain-boundary bulging also recorded in these samples would indicate lower deformation temperatures (390–420 °C), possibly reflecting later stages of deformation and exhumation (cf. Law *et al.* 2013). Samples that exhibit dominantly prism <a> slip with minor rhomb <a> and basal <a> slip based on fabric topology (Fig. 5) have microstructures suggesting grain-boundary migration recrystallization and opening angles that indicate deformation temperatures of 500–630 °C. Although, the skeletal topology of these quartz fabrics was interpreted as indicating a progressively increasing contribution of prism <a> slip, relative to basal <a> and rhomb <a> slip, with increasing distance above the Sirjan thrust fault, it may be suggested that the observed spatial variations in microstructures and fabric opening angles are a reflection of increasing hydrolytic weakening and decreasing strain rate traced away from the fault surface (Law, 2014). Unfortunately, no analytical criteria are available for assessing the influence of strain rate on fabric development and recrystallization regime that are independent of deformation temperature and hydrolytic weakening (Law *et al.* 2013; Law, 2014). Assuming an average geothermal gradient of 30 °C km^{-1}, the Sirjan thrust was deformed at a maximum crustal depth of ~ 21 km based on our estimated deformation temperatures. Therefore, the shear zone located along the base of the Sirjan thrust sheet was initiated at mid-crustal levels in a contractional tectonic regime.

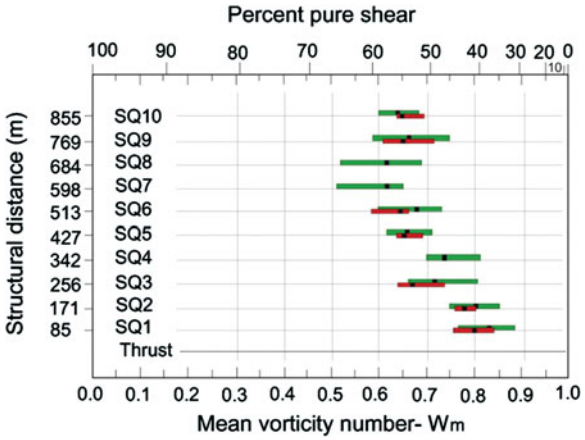

Figure 12. (Colour online) Bar chart of vorticity numbers calculated by Method I (green bars; top) and Method II (red bars; bottom) versus structural distance from the Sirjan thrust; length of bars reflects the uncertainty in the calculation of W_m values. For further details see Table 1. Black rectangles on bars indicate W_m values for best-fit β-value (Fig. 6).

8.b. Kinematic vorticity profiles

The results of the vorticity analysis for each sample were plotted against structural distance from the thrust plane to examine the spatial variation of W_m values within the deformation zone as well as analytical consistency between the two methods (Fig. 12). In Figure 12 the length of each bar indicates the degree

https://doi.org/10.1017/S0016756815000941 Published online by Cambridge University Press

of uncertainty in the input data. It is clear that both methods record a consistent pattern of vorticity distribution along the sampling transect; however, there is a greater degree of uncertainty in estimating W_m values using Method I in comparison with Method II. Moreover, within individual samples, Method I generally indicates higher W_m values than those obtained by Method II.

The majority of samples from the sampling transect, yield W_m estimates in the 0.51 and 0.89 range (31–60 % pure shear) using the R_{xz}/β-method (n = 10), and 0.6–0.84 (36–63 % pure shear) using the oblique quartz grain shape foliation method (n = 7). These results indicate a spatial variation in deformation during exhumation, in which simple shear dominated deformation near the thrust, and pure shear dominated deformation at greater distances above the thrust. Vorticity estimates derived from the R_{xz}/β-method record a higher component of simple shear than estimates derived from the δ/β-method (Fig. 12). Wallis (1995) interpreted a similar mismatch between the W_m values obtained using these two methods to reflect a change of flow regime with time, and suggested that Method II may record the final increments of deformation.

Our observations indicate that the deformation history of rocks in the Sirjan thrust sheet is characterized by higher W_m values ($\sim$ 0.89) close to the thrust plane, which systematically decrease towards the middle parts of the overlying thrust sheet reaching a value of $\sim$ 0.6 at a structural distance of 513 m above the thrust plane. Given the above discussion, comparison between W_m estimates obtained from methods I and II suggests that Method I may overestimate the simple shear component close to the thrust plane.

8.c. Mid-crustal exhumation/extrusion of the Sirjan thrust sheet

There is a wealth of field data showing key characteristics of crustal extrusion, including (Fig. 13): (1) high-grade units in the core of the thrust sheet, with inverted metamorphism across the lower margin of the fault zone; (2) evidence of partial melting, marked by younger ages in the centre of the sheet; (3) active deformation synchronous with crystallization of anatectic melts; (4) ductile fabrics progressively overprinted by semi-ductile and brittle structures; and (5) sub-simple shear strains, with a large component of up-dip stretching (cf. criteria described by Jones *et al.* 2006).

In the study area the thrust sheet is exposed in a large asymmetric structural window and consists of gneissic basement rocks of the Arabian continent that have been extruded as a mylonitic thrust sheet. Small domes of leucogranite observed in the inner part of the thrust sheet are the result of anatectic melting. Thrusting along the eastern margin of the thrust sheet has resulted in emplacement of quartzo-feldspathic gneiss rock over relatively low-grade metamorphic rocks (Fig. 3a). Subhorizontal to shallowly plunging stretching lineations, moderately mylonitic foliations (Fig. 2) and semi-quantitative analysis of quartz fabrics (Fig. 5) from quartz-rich mylonite within the Sirjan thrust sheet demonstrate plane strain deformation under amphibolite- to granulite-facies conditions. Semi-brittle and ductile kinematic indicators including mylonitic gneiss with well-developed shear sense indicators such as domino-like structures with antithetic micro-faults transecting K-feldspar (Fig. 4d), rotated porphyroclasts, mica fish (Figs 3c, 7) and quartz c-axis patterns (Fig. 5) suggest a top-to-the-SW sense of shear.

Detailed fabric analysis of the preferred orientation of quartz c-axes indicates that this pervasive ductile deformation is characterized by heterogeneous general non-coaxial flow with components of simple and pure shear that formed in a sub-simple shear zone. The estimated kinematic vorticity (W_k) values indicate a 32–59 % pure shear component and a 41–68 % simple shear component. Moreover, quantitative vorticity analyses within quartzo-feldspathic gneisses of the Sirjan thrust sheet document a progressively increasing component of simple shear traced downwards towards the thrust plane (Fig. 12). The occurrence of strike-slip and oblique-slip deformation with a strong component of pure shear, confirms transpressional deformation (Sanderson & Marchini, 1984; Tikoff & Teyssier, 1994). Several structural studies of deformation patterns imply a transpressional regime within the Sanandaj–Sirjan metamorphic belt (Mohajjel & Fergusson, 2000; Sarkarinejad, Faghih & Grasemann, 2008; Sarkarinejad & Azizi, 2008; Sarkarinejad, Godin & Faghih, 2009), which show numerous shear zones accommodating deformation and exhumation of medium- to high-grade metamorphic rocks during oblique collision between the Afro-Arabian continent and the Iranian microcontinents.

Structural studies around the margins of the thrust sheet reveal a protracted kinematic history in which earlier ductile (crystal plastic) fabrics are generally overprinted by later brittle-ductile structures. The sequence of ductile and brittle structures now visible at the ground surface documents progressive exhumation. The western margin of the quartzo-feldspathic gneisses preserved in the thrust sheet is not as widely studied or well understood as the eastern margin. Further field work is clearly needed to provide additional constraints on the kinematics of deformation on the western margin. Available data indicate that the western margin of the thrust sheet is dominated by ductile deformation with little brittle deformation, while the eastern margin near to the thrust fault is characterized by ductile to brittle deformation.

8.d. Comparison with ductile shear zones from other orogens

The exhumation of the Sirjan gneissic thrust sheet and the associated pattern of spatial variations in deformation temperature and kinematics of flow are similar to what has been observed in: (1) the hanging wall to the

https://doi.org/10.1017/S0016756815000941 Published online by Cambridge University Press

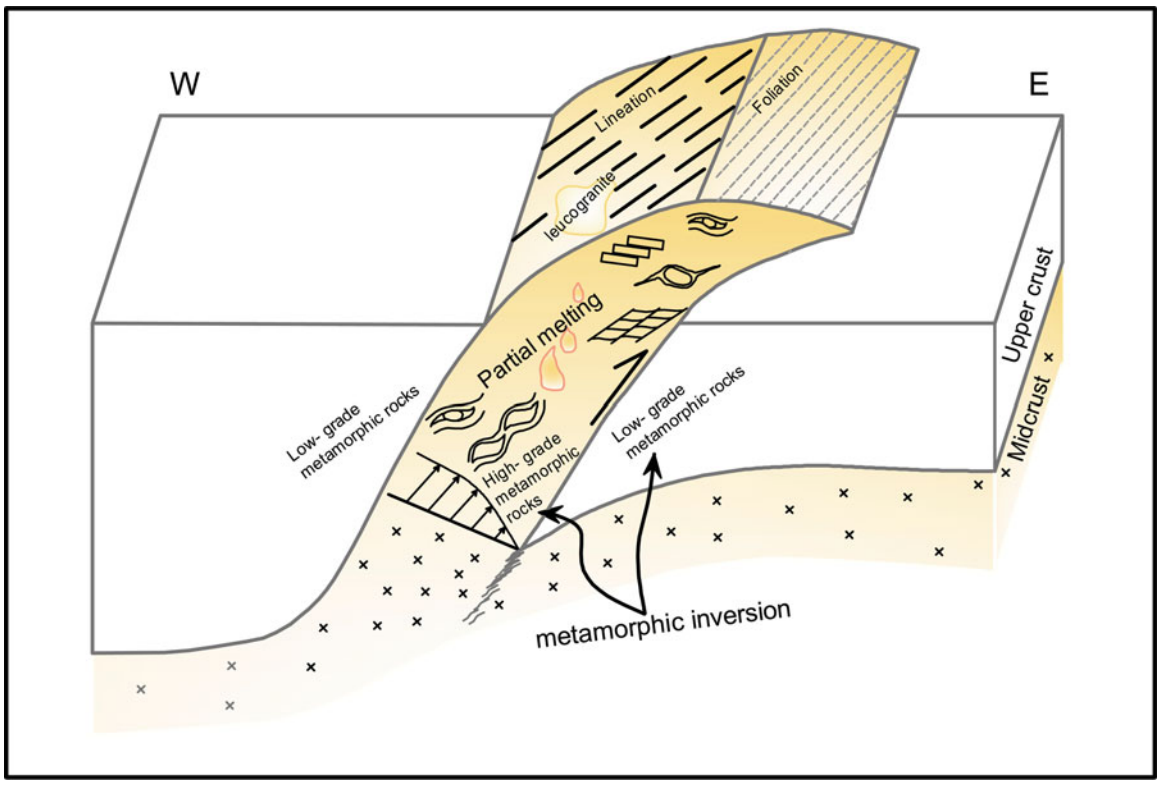

Figure 13. (Colour online) Schematic diagram of the deformation pattern in the Sirjan thrust sheet. The occurrence of inversion metamorphism, partial melting, ductile fabrics progressively overprinted by semi-ductile and brittle structures and sub-simple shear strains with a large component of up-dip stretching reveals the extrusion mechanism for this thrust sheet. The length of the arrows indicates the value of pure shear in the deformation across the thrust sheet (for details see text).

Main Central Thrust in the Sutlej Valley and Shimla Klippe of the western Himalaya (Law *et al.* 2013); (2) the footwall to the Moine thrust at the Stack of Glencoul in the Assynt region of NW Scotland (Law *et al.* 2010; Law, 2010); (3) the footwall to the South Tibetan Detachment System in the Mount Everest Massif of Tibet/Nepal (Law, Searle & Simpson, 2004; Jessup *et al.* 2006); (4) the Ama Drime Massif southern Tibet (Langille *et al.* 2010); and (5) the Ochi nappe in the Alpine orogenic belt of Greece (Xypolias *et al.* 2010), which is characterized by a progressive reduction in simple shear traced from the base to the centre of the deformation zone (e.g. Xypolias *et al.* 2010).

The estimated deformation temperature indicated by quartz recrystallization microstructures and c-axis fabric opening angles in the study area is similar to the ranges of deformation temperatures estimated for Himalayan gneissic shear zones (e.g. Célérier *et al.* 2009; Law *et al.* 2010, 2013; Langille *et al.* 2010). For example, deformation temperatures indicated by fabric opening angles at 20–75 m above the Main Central Thrust are estimated at 535–550 and 610 °C on the Sutlej and Eastern Sutlej transects, respectively. These temperatures steadily increase non-linearly up structural section, reaching 615 °C at 1150 m above the Main Central Thrust on the Sutlej transect and 680 °C at 2200 m above the Main Central Thrust on the Eastern Sutlej transect (Law *et al.* 2013). Also, in the Kangmar gneiss dome of southern Tibet, deformation temperatures inferred from grain-scale microstructures and quartz lattice preferred orientations increase from 300–400 °C to ≥ 600 °C in the deepest exposed rocks (Wagner *et al.* 2010).

The observed increase in R_{xz} strain ratios from 2.5 at the top of the Sirjan gneissic thrust sheet to 4.3 at the base is comparable with strain variations recorded within other ductile shear zones. For instance, low R_{xz} strain ratios of ~ 3 to 6.43 and 4.9 to 8.22 have been recorded at the uppermost structural levels of the Eva and Ochi thrust zones, respectively (Xypolias *et al.* 2010), and high strain ratios, possibly up to 20, have been recorded close to the Main Central Thrust in the Sutlej Valley of NW India (Grasemann, Fritz & Vannay, 1999). Moreover, an overall downward increase in strain increase is at least locally documented for rocks in the hanging wall of the Main Central Thrust Zone by the intensity of the lattice preferred orientation of quartz c-axis fabrics (e.g. Bhattacharya & Weber, 2004). The strain magnitude within the HP nappe of the Penninic Alps is also considered to increase downwards from a value of 2.0–6.0 at the top to an extremely high value (*c.* 30) near the base (Escher & Beaumont, 1997; Xypolias & Kokkalas, 2006).

9. Conclusion

A new study of quartz recrystallization microstructures and c-axis fabrics preserved in rocks from the hanging wall of the Sirjan thrust sheet suggests that these rocks record a top-to-the-SW sense of shear.

https://doi.org/10.1017/S0016756815000941 Published online by Cambridge University Press

Quantitative finite strain and vorticity analyses demonstrated that both the strain ratio and the kinematic vorticity number increase towards the underlying Sirjan thrust. The estimated mean kinematic vorticity number (W_m) based on quartz fabrics indicates deformation occurred under general shear conditions (W_m values of 0.6–0.89) with contemporaneous contributions of pure (32–59 %) and simple shear(41–68 %). Deformation temperatures (430 to 625 ± 50 °C) inferred from fabric opening angles are in good agreement with likely ranges of deformation temperatures indicated by quartz recrystallization microstructures within individual samples. The observed spatial variation in strain and vorticity and deformation temperature within the study area is comparable with patterns recorded within other hinterlandward-located basement rocks of the world's orogenic belts.

Acknowledgements. The authors are grateful to Professor Mark Allen for his editorial authority. We would like to thank Professor Richard Law, for critical reading/editing of the manuscript, which helped to considerably improve the scientific content and presentation of the manuscript. We are grateful to Paris Xypolias, Chiara Frassi and Enrique Gomez-Rivas for their constructive comments, which greatly improved the earlier version of the manuscript. The Research Council of Shiraz University has supported this work, which is gratefully acknowledged.

References

AGARD, P., OMRANI, J., JOLIVET, L. & MOUTHEREAU, F. 2005. Convergence history across Zagros (Iran): constraints from collisional and earlier deformation. *International Journal of Earth Sciences* **94**, 401–19.

ALAVI, M. 1994. Tectonics of the Zagros orogenic belt of Iran: new data and interpretations. *Tectonophysics* **229**, 211–38.

ALIZADEH, A., LÓPEZ-MARTÍNEZ, M. & SARKARINEJAD, K. 2010. ^{40}Ar–^{39}Ar geochronology in a gneiss dome within the Zagros Orogénic Belt. *Comptes Rendus Geoscience* **342**, 837–84.

ALLEN, M., JACKSON, J. & WALKER, R. 2004. Late Cenozoic reorganization of the Arabia–Eurasia collision and the comparison of short-term and long-term deformation rates. *Tectonics* **23**, 1–16.

BAILEY, C. M. & EYSTER, E. L. 2003. General shear deformation in the Pinaleno Mountains metamorphic core complex, Arizona. *Journal of Structural Geology* **25**, 1883–92.

BAILEY, C. M., FRANCIS, B. E. & FAHRNEY, E. E. 2004. Strain and vorticity analysis of transpressional high-strain zones from the Virginia Piedmont, USA. In *Flow Processes in Faults and Shear Zones* (eds G. I. Alsop, R. E. Holdsworth, K. J. W. McCaffrey & M. Hand), pp. 249–64. Geological Society of London, Special Publication no. 224.

BERBERIAN, M. & KING, G. C. P. 1981. Towards a paleogeography and tectonic evolution of Iran. *Canadian Journal of Earth Sciences* **18**, 210–65.

BHATTACHARYA, A. R. & WEBER, K. 2004. Fabric development during shear deformation in the Main Central Thrust Zone, NW-Himalaya, India. *Tectonophysics* **387**, 23–46.

BLANC, E. J.-P., ALLEN, M. B., INGER, S. & HASSANI, H. 2003. Structural styles in the Zagros simple folded zone, Iran. *Journal of Structural Geology* **160**, 401–12.

BOUCHEZ, J. L. 1977. Plastic deformation of quartzites at low temperatures in an area of natural strain gradient. *Tectonophysics* **39**, 25–50.

BOUCHEZ, J. L. & DUVAL, P. 1982. The fabric of polycrystalline ice deformed in simple shear: experiments in torsion, natural deformation and geometrical interpretation. *Textures and Microstructures* **5**, 171–90.

BOUCHEZ, J. L. & PECHER, A. 1981. The Himalayan Main Central Thrust pile and its quartz-rich tectonites in central Nepal. *Tectonophysics* **78**, 23–50.

BURG, J. P. 1986. Quartz shape fabric variations and c-axis fabrics in a ribbon mylonite: arguments for an oscillating foliation. *Journal of Structural Geology* **8**, 123–31.

CAVALCANTI DE ARAÚJO, M. N., ALVES DA SILVA, F. C., JARDIM DE SÁ, E. F., HOLCOMBE, R. J. & DE VASCONCELOS, P. M. 2003. Microstructural evolution of the Seridó Belt, NE Brazil: the effect of two tectonic events on development of c-axis preferred orientation in quartz. *Journal of Structural Geology* **25**, 2089–107.

CÉLÉRIER, J., HARRISON, T. M., BEYSSAC, O., HERMAN, F., DUNLAP, W. J. & WEBB, A. G. 2009. Evolution of the Kumaun and Garwhal Lesser Himalaya, India. Part 2: thermal and deformation histories. *Geological Society of American Bulletin* **121**, 1281–97.

CHEW, D. M. 2003. An Excel spreadsheet for finite strain analysis using the Rf/Φ technique. *Computers and Geosciences* **29**, 795–99.

DEWEY, J. F., PITMAN III, W. C., RYAN, W. B. F. & BONINI, J. 1973. Plate tectonics and the evolution of the Alpine System. *Geological Society of America Bulletin* **84**, 3137–80.

ESCHER, A. & BEAUMONT, C. 1997. Formation, burial and exhumation of basement nappes at crustal scale: a geometric model based on the Western Swiss-Italian Alps. *Journal of Structural Geology* **19**, 955–74.

ETCHECOPAR, A. & VASSEUR, G. 1987. A 3D kinematic model of fabric development in polycrystalline aggregates: comparisons with experimental and natural examples. *Journal of Structural Geology* **9**, 705–17.

FAGHIH, A. & SOLEIMANI, M. 2015. Quartz c-axis fabric development associated with shear deformation along an extensional detachment shear zone: Chapedony Metamorphic Core Complex, Central-East Iranian Microcontinent. *Journal of Structural Geology* **70**, 1–11.

FITZ GERALD, J. D. & STÜNITZ, H. 1993. Deformation of granitoids at low metamorphic grades. I: reactions and grain size reduction. *Tectonophysics* **221**, 269–97.

FRASSI, C., CAROSI, R., MONTOMOLI, C. & LAW, R. D. 2009. Kinematics and vorticity of flow associated with post-collisional oblique transpression in the Variscan Inner Zone of northern Sardinia (Italy). *Journal of Structural Geology* **31**, 1458–71.

GHASEMI, A. & TALBOT, C. J. 2006. A new tectonic scenario for the Sanandaj–Sirjan Zone (Iran). *Journal of Asian Earth Science* **26**, 683–93.

GOMEZ-RIVAS, E., BONS, P. D., GRIERA, A., CARRERAS, J., DRUGUET, E. & EVANS, L. 2007. Strain vorticity analysis using small-scale faults and associated drag folds. *Journal of Structural Geology* **29**, 1882–99.

GOSCOMBE, B. & PASSCHIER, C. W. 2003. Asymmetric boudins as shear sense indicators—an assessment from field data. *Journal of Structural Geology* **25**, 575–89.

GOSCOMBE, B., PASSCHIER, C. W. & HAND, M. 2004. Boudinage classification: end member boudin types and

modified boudin structures. *Journal of Structural Geology* **26**, 739–63.

GRASEMANN, B., FRITZ, H. & VANNAY, J. C. 1999. Quantitative kinematic flow analysis from the Main Central Thrust Zone (NW-Himalaya, India): implications for a decelerating strain path and the extrusion of orogenic wedges. *Journal of Structural Geology* **21**, 837–53.

GRUJIC, D., CASEY, M., DAVIDSON, C., HOLLISTER, L. S., KUNDIG, R., PAVLIS, T. & SCHMID, S. 1996. Ductile extrusion of the Higher Himalayan Crystalline in Bhutan: evidence from the quartz microfabrics. *Tectonophysics* **260**, 21–43.

HANMER, S. & PASSCHIER, C. 1991. Shear-sense indicators: a review. Geological Survey of Canada, Paper 90–17, 72 pp.

HERWEGH, M. & HANDY, M. R. 1996. The evolution of high temperature mylonitic microfabrics: evidence for simple shearing of a quartz analogue (norcamphor). *Journal of Structural Geology* **18**, 689–710.

HERWEGH, M., HANDY, M. R. & HEILBRONNER, R. 1997. Temperature- and strain rate-dependent microfabric evolution in monomineralic mylonite: evidence from in-situ deformation of norcamphor. *Tectonophysics* **280**, 83–106.

HIRTH, G., TEYSSIER, C. & DUNLAP, W. J. 2001. An evaluation of quartzite flow laws based on comparisons between experimentally and naturally deformed rocks. *International Journal of Earth Sciences* **90**, 77–87.

HIRTH, G. & TULLIS, J. 1992. Dislocation creep regimes in quartz aggregates. *Journal of Structural Geology* **14**, 145–59.

HOLCOMBE, R. J. & LITTLE, T. A. 2001. A sensitive vorticity gauge using rotated prophyroblasts, and its application to rocks adjacent to the Alpine fault, New Zealand. *Journal of Structural Geology* **23**, 979–89.

HUBBARD, M. 1996. Ductile shear as a cause of inverted metamorphism: example from the Nepal Himalaya. *Journal of Geology* **104**, 493–99.

HUBBARD, M. 1997. Ductile shear as a cause of inverted metamorphism: example from the Nepal Himalaya: a reply. *Journal of Geology* **105**, 513–4.

JACKSON, J. A. & MCKENZIE, D. P. 1984. Active tectonics of Alpine–Himalayan belt between western Turkey and Pakistan. *Geophysical Journal of the Royal Astronomical Society* **77**, 185–264.

JAIN, A. K. & MANICKAVASAGAM, R. M. 1993. Inverted metamorphism in the intercontinental ductile shear zone during Himalayan collision tectonics. *Geology* **21**, 407–10.

JAIN, A. K. & MANICKAVASAGAM, R. M. 1997. Ductile shear as a cause of inverted metamorphism: example from the Nepal Himalaya: a discussion. *Journal of Geology* **105**, 511–3.

JESSELL, M. W. 1987. Grain-boundary migration microstructures in a naturally deformed quartzite. *Journal of Structural Geology* **9**, 1007–14.

JESSUP, M. J., LAW, R. D. & FRASSI, C. 2007. The Rigid Grain Net (RGN): an alternative method for estimating mean kinematic vorticity number (W_m). *Journal of Structural Geology* **29**, 411–21.

JESSUP, M. J., LAW, R. D., SEARLE, M. P. & HUBBARD, M. S. 2006. Structural evolution and vorticity of flow during extrusion and exhumation of the Greater Himalayan Slab, Mount Everest massif, Tibet/Nepal: implications for orogen-scale flow partitioning. In *Channel Flow, Ductile Extrusion and Exhumation in Continental Collision Zones* (eds R. Law, M. P. Searle & L. Godin), pp. 379–414. Geological Society of London, Special Publications no. 268.

JONES, R. R., HOLDSWORTH, R. E., HAND, M. & GOSCOMBE, B. 2006. Ductile extrusion in continental collision zones: ambiguities in the definition of channel flow and its identification in ancient orogens. In *Channel Flow, Ductile Extrusion and Exhumation in Continental Collision Zones* (eds R. D. Law, M. P. Searle & L. Godin), pp. 201–19. Geological Society of London, Special Publications no. 268.

KLEPEIS, K. A., DACZKO, N. R. & CLARKE, G. L. 1999. Kinematic vorticity and tectonic significance of superposed mylonites in a major lower crustal shear zone, northern Fiordland, New Zealand. *Journal of Structural Geology* **21**, 1385–406.

KRUHL, J. H. 1996. Prism- and basal-plane parallel subgrain boundaries in quartz: a microstructural geothermobarometer. *Journal of Metamorphic Geology* **14**, 581–9.

KRUHL, J. H. 1998. Reply: Prism- and basal-plane parallel subgrain boundaries in quartz: a microstructural geothermobarometer. *Journal of Metamorphic Geology* **16**, 142–6.

LANGILLE, J., JESSUP, M. J., COTTLE, J. M. & NEWELL, D. L. 2010. Kinematics of the Ama Drime Detachment: insights into orogen-parallel extension and exhumation of the Ama Drime Massif, Tibet–Nepal. *Journal of Structural Geology* **32**, 900–19.

LAW, R. D. 1987. Heterogeneous deformation and quartz crystallographic fabric transitions: natural examples from the Moine thrust zone at the Stack of Glencoul, northern Assynt. *Journal of Structural Geology* **9**, 819–34.

LAW, R. D. 1990. Crystallographic fabrics: a selective review of their applications to research in structural geology. In *Deformation Mechanisms, Rheology and Tectonics* (eds R. J. Knipe & E. H. Rutter), pp. 335–52. Geological Society of London, Special Publication no. 54.

LAW, R. D. 2010. Moine Thrust zone mylonites at the Stack of Glencoul: II – results of vorticity analyses and their tectonic significance. In *Continental Tectonics and Mountain Building* (eds R. D. Law, R. Butler, B. Holdsworth, M. Krabbendam & R. Strachan), pp. 579–602. The Legacy of Peach and Horne; Geological Society of London, Special Publication no. 335.

LAW, R. D. 2014. Deformation thermometry based on quartz c-axis fabrics and recrystallization microstructures: a review. *Journal of Structural Geology* **66**, 129–61.

LAW, R. D., CASEY, M. & KNIPE, R. J. 1986. Kinematic and tectonic significance of microstructures and crystallographic fabrics within quartz mylonites from the Assynt and Eriboll regions of the Moine thrust zone, NW Scotland. *Transactions of the Royal Society of Edinburgh: Earth Sciences* **77**, 99–126.

LAW, R. D., KNIPE, R. J. & DAYAN, H. 1984. Strain path partitioning within thrust sheets: microstructural and petrofabric evidence from the Moine thrust zone at Loch Eriboll, NW Scotland. *Journal of Structural Geology* **6**, 477–97.

LAW, R. D., MAINPRICE, D. H., CASEY, M., LLOYD, G. E., KNIPE, R. J., COOK, B. & THIGPEN, J. R. 2010. Moine thrust zone mylonites at the Stack of Glencoul: I – microstructures, strain and influence of recrystallization on quartz crystal fabric development. In *Continental Tectonics and Mountain Building* (eds R. D. Law, R. Butler, B. Holdsworth, M. Krabbendam & R. Strachan), pp. 543–77. The Legacy of Peach and Horne; Geological Society of London, Special Publication no. 335.

LAW, R. D., MORGAN, S. S., CASEY, M., SYLVESTER, A. G. & NYMAN, M. 1992. The Papoose Flat pluton of eastern California: a re-assessment of its emplacement history

in the light of new microstructural and crystallographic fabric observations. *Transactions of the Royal Society of Edinburgh: Earth Sciences* **83**, 361–75.

LAW, R. D., SEARLE, M. P. & SIMPSON, R. L. 2004. Strain, deformation temperatures and vorticity of flow at the top of the Greater Himalayan Slab, Everest Massif. Tibet. *Journal of Geological Society, London* **161**, 305–20.

LAW, R. D., STAHR, D. W., FRANCSIS, M., ASHLEY, K. T., GRASEMANN, B. & AHMAD, T. 2013. Deformation temperatures and flow vorticities near the base of the Greater Himalayan Series, Sutlej Valley and Shimla Klippe, NW India. *Journal of Structural Geology* **54**, 21–53.

LIN, S., JIANG, D. & WILLIAMS, P. F. 1998. Transpression (or transtension) zones of triclinic symmetry: natural example and theoretical modelling. In: *Continental Transpressional and Transtensional Tectonics* (eds R. E. Holdsworth, R. A. Strachan & J. F. Dewey), pp. 41–57. Geological Society of London, Special Publication no. 135.

LLOYD, G. E. & FREEMAN, B. 1994. Dynamic recrystallization of quartz under greenschist conditions. *Journal of Structural Geology* **16**, 867–81.

LISLE, R. J. 1985. *Geological Strain Analysis: A Manual for the R_f/Φ Method*. New York: Pergamon Press, 99 pp.

LISTER, G. S. 1977. Discussion: crossed-girdle c-axis fabrics in quartzites plastically deformed by plane strain and progressive simple shear. *Tectonophysics* **39**, 51–4.

LISTER, G. S. & DORNSIEPEN, U. F. 1982. Fabric transitions in the Saxony granulite terrain. *Journal of Structural Geology* **4**, 81–92.

LISTER, G. S. & HOBBS, B. E. 1980. The simulation of fabric development during plastic deformation and its application to quartzite: fabric transition. *Journal of Structural Geology* **1**, 99–115.

LISTER, G. S. & SNOKE, A. W. 1984. S–C mylonites. *Journal of Structural Geology* **6**, 616–38.

LISTER, G. S. & WILLIAMS, P. F. 1979. Fabric development in shear zones: theoretical controls and observed phenomena. *Journal of Structural Geology* **1**, 283–98.

MAINPRICE, D., BOUCHEZ, J. L., BLUMENFELD, P. & TUBIA, J. M. 1986. Dominant c slip in naturally deformed quartz: implications for dramatic plastic softening at high temperature. *Geology* **14**, 819–22.

MCCALL, G. J. H. & KIDD, R. G. W. 1981. The Makran, southeastern Iran: the anatomy of a converging plate margin active from Cretaceous to Present. In: *Trench–Fore Arc Geology* (eds J. Leggett), pp. 387–97. Geological Society of London, Special Publications no. 10.

MEANS, W. D. 1994. Rotational quantities in homogeneous flow and development of small-scale structures. *Geology* **16**, 437–46.

MOHAJJEL, M. & FERGUSSON, C. L. 2000. Dextral transpression in Late Cretaceous continental collision, Sanandaj Sirjan Zone, western Iran. *Journal of Structural Geology* **22**, 1125–39.

MOHAJJEL, M., FERGUSSON, C. L. & SAHANDI, M. R. 2003. Cretaceous–Tertiary convergence and continental collision, Sanandaj–Sirjan Zone, western Iran. *Journal of Asian Earth Sciences* **21**, 397–412.

MORGAN, S. S. & LAW, R. D. 2004. Unusual transition in quartzite dislocation creep regimes and crystal slip systems in the aureole of the Eureka Valley–Joshua Flat–Beer Creek pluton, California: a case for anhydrous conditions created by decarbonation reactions. *Tectonophysics* **384**, 209–31.

MOUTHEREAU, F., LACOMBE, O., TENSI, J., BELLAHSEN, N., KARGAR, S. & AMROUCH, K. 2007. Mechanical constraints on the development of the Zagros Folded Belt (Fars). In *Thrust Belts and Foreland Basins: From Fold Kinematics to hydrocarbon Systems* (eds O. Lacombe, J. Lavé, F. Roure & J. Vergés), pp. 245–64. Berlin, Heidelberg: Springer-Verlag.

NYMAN, M. W., LAW, R. D. & MORGAN, S. S. 1995. Conditions of contact metamorphism, Papoose Flat Pluton, eastern California, USA: implications for cooling and strain histories. *Journal of Metamorphic Geology* **13**, 627–43.

OKUDAIRA, T., TAKESHITA, T., HARA, I. & ANDO, J. 1995. A new estimate of the conditions for transition from basal <a> to prism [c] slip in naturally deformed quartz. *Tectonophysics* **250**, 31–46.

PAMPLONA, J. & RODRIGUES, B. 2011. Kinematic interpretation of shearband boudins: new parameters and ratios useful in HT simple shear zones. *Journal of Structural Geology* **33**, 38–50.

PASSCHIER, C. W. 1987. Stable positions of rigid objects in non-coaxial flow: a study in vorticity analysis. *Journal of Structural Geology* **9**, 679–90.

PASSCHIER, C. W. 1988. Analysis of deformation paths in shear zones. *Geologische Rundschau* **77**, 309–18.

PASSCHIER, C. W. 1998. Monoclinic model shear zone. *Journal of Structural Geology* **20**, 1121–37.

PASSCHIER, C. W. & SIMPSON, C. 1986. Porphyroclast systems as kinematic indicators. *Journal of Structural Geology* **8**, 831–43.

PASSCHIER, C. W. & TROUW, R. A. J. 2005. *Microtectonics*. Berlin: Springer, 366 pp.

PLATT, J. P. & BEHRMANN, J. H. 1986. Structures and fabrics in a crustal scale shear zone, Betic Cordilleras, S.E. Spain. *Journal of Structural Geology* **8**, 15–34.

RAMSAY, J. G. & HUBER, M. I. 1983. *The Techniques of Modern Structural Geology. Volume 1: Strain Analysis*. London: Academic Press, 307 pp.

RATSCHBACHER, L., WENK, R. H. & SINTUBIN, M. 1991. Calcite textures: examples from nappes with strain-path partitioning. *Journal of Structural Geology* **13**, 369–84.

REGARD, V., BOLLIER, O., THOMAS, J. C., ABBASI, M. R., MERCIER, J., SHABANIAN, E., FEGHHI, K. & SOLEYMANI, S. 2004. Accommodation of Arabia–Eurasia convergence in the Zagros–Makran transfer zone, SE Iran: a transition between collision and subduction through a young deformation system. *Tectonics* **23**, TC4007, doi: 10.1029/2003TC001599.

RICOU, L. E. 1971. Le croissant ophiolitique péri-arabe. Une ceinture de nappes mises en place au Crétacé supérieur. *Revue de Géographie Physique et de Géologie Dynamique* **XIII**, 327–50.

SAMANI, B. 2013. Quartz c-axis evidence for deformation characteristics in the Sanandaj–Sirjan metamorphic belt, Iran. *Journal of African Earth Sciences* **81**, 28–34.

SANDERSON, D. J. & MARCHINI, W. R. D. 1984. Transpression. *Journal of Structural Geology* **6**, 449–58.

SARKARINEJAD, K. 1999. Tectonic finite strain analysis using Ghouri deformed conglomerate, Neyriz area, Southwestern Iran. *Iranian Journal of Science and Technology* **23**, 352–63.

SARKARINEJAD, K. 2005. Structures and microstructures related to steady-state mantle flow in the Neyriz ophiolite, Iran. *Journal of Asian Earth Sciences* **25**, 859–81.

SARKARINEJAD, K. 2007. Quantitative finite strain and kinematic flow analyses along the Zagros transpression zone, Iran. *Tectonophysics* **442**, 49–65.

SARKARINEJAD, K. & AZIZI, A. 2008. Slip partitioning and inclined dextral transpression along the Zagros Thrust System, Iran. *Journal of Structural Geology* **30**, 116–36.

SARKARINEJAD, K., FAGHIH, A. & GRASEMANN, B. 2008. Transpressional deformations within the Sanandaj–Sirjan Metamorphic Belt (Zagros Mountains, Iran). *Journal of Structural Geology* **30**, 818–26.

SARKARINEJAD, K. & GHANBARIAN, M. A. 2014. The Zagros hinterland fold-and-thrust belt in-sequence thrusting, Iran. *Journal of Asian Earth Sciences* **85**, 66–79.

SARKARINEJAD, K., GODIN, L. & FAGHIH, A. 2009. Kinematic vorticity flow analysis and $^{40}Ar/^{39}Ar$ geochronology related to inclined extrusion of the HP–LT metamorphic rocks along the Zagros accretionary prism, Iran. *Journal of Structural Geology* **31**, 691–706.

SARKARINEJAD, K. & KESHAVARZ, S. 2015. Quantitative kinematic analysis of the asymmetric boudins of the Zagros accretionary prism, Iran. *Geosciences Journal* **19**, 415–30.

SARKARINEJAD, K., PARTABIAN, A. & FAGHIH, A. 2013. Variations in the kinematics of deformation along the Zagros inclined transpression zone, Iran: implications for defining a curved inclined transpression zone. *Journal of Structural Geology* **48**, 126–36.

SCHMID, S. M. & CASEY, M. 1986. Complete fabric analysis of some commonly observed quartz c-axis patterns. In *Mineral and Rock Deformation: Laboratory Studies – The Paterson Volume* (eds B. E. Hobbs & H. C. Heard), pp. 263–86. American Geophysical Union, Geophysical Monograph vol. 36. Washington, DC, USA.

SENGÖR, A. M. C., ALTINER, D., CIN, A., CUSTAOMER, T. & HSU, K. J. 1988. Origin and assembly of the Tethyside orogenic collage at the expense of Gondwana Land. In *Gondwana and Tethys* (eds M. G. Audley-Charles & A. Hallam), pp. 119–81. Geological Society of London, Special Publication no. 37.

SHEIKHOLESLAMI, M. R., PIQUE, A., MOBAYEN, P., SABZEHEI, M., BELLON, H. & HASHEM EMAMI, M. 2008. Tectono-metamorphic evolution of the Neyriz metamorphic complex, Quri-Kor-e-Sefid area (Sanandaj–Sirjan Zone, SW Iran). *Journal of Asian Earth Sciences* **31**, 504–21.

SIMPSON, C. & DE PAOR, D. G. 1997. Practical analysis of general shear zones using the porphyroclast hyperbolic distribution method: an example from Scandinavian Caledonides. In *Evolution of Geological Structures in Micro to Macro Scales* (eds S. Sengupta), pp. 169–84. London: Chapman and Hall.

SIMPSON, C. & SCHMID, S. M. 1983. An evaluation of criteria to deduce the sense of movement in sheared rocks. *Geological Society of America Bulletin* **94**, 1281–8.

STIPP, M., STUNITZ, H., HEILBRONNER, R. & SCHMID, S. M. 2002*a*. The eastern Tonale fault zone: a 'natural laboratory' for crystal plastic deformation of quartz over a temperature range from 250 to 700 ºC. *Journal of Structural Geology* **24**, 1861–84.

STIPP, M., STÜNITZ, H., HEILBRONNER, R. & SCHMID, S. M. 2002*b*. Dynamic recrystallization of quartz: correlation between natural and experimental conditions. In *Deformation Mechanisms, Rheology and Tectonics: Current Status and Future Perspectives* (eds S. De Meer, M. R. Drury, J. H. P. De Bresser & G. M. Pennock), pp. 171–90. Geological Society of London, Special Publication no. 200.

STÖCKLIN, J. 1968. Structural history and tectonics of Iran: a review. *American Association of Petroleum Geologists Bulletin*, **52**, 1229–58.

STÖCKLIN, J. 1974. Possible ancient continental margins in Iran. In *The Geology of Continental Margins* (eds C. A. Burk & C. L. Drake), pp. 873–88. New York: Springer.

SULLIVAN, W. A. 2008. Significance of transport-parallel strain variations in part of the Raft River shear zone, Raft River Mountains, Utah, USA. *Journal of Structural Geology* **30**, 138–58.

SULLIVAN, W. A. & LAW, R. D. 2007. Deformation path partitioning within the transpressional White Mountain shear zone, California and Nevada. *Journal of Structural Geology* **29**, 583–98.

TATAR, M., HATZFELD, D. & GHAFORY-ASHTIYANI, M. 2004. Tectonics of the Central Zagros (Iran) deduced from microearthquake seismicity. *Geophysical Journal International* **156**, 255–66.

TIKOFF, B. & FOSSEN, H. 1995. The limitation of three-dimensional kinematic vorticity analysis. *Journal of Structural Geology* **17**, 1771–84.

TIKOFF, B. & TEYSSIER, C. 1994. Strain and fabric based on porphyroclast interaction. *Journal of Structural Geology* **16**, 477–91.

TULLIS, J. & YUND, R. A. 1992. The brittle-ductile transition in feldspar aggregates; an experimental study. In *Fault Mechanics and Transport Properties in Rocks* (eds B. Evans & T. F. Wong), pp. 89–118. New York: Academic Press.

VERNANT, P., NILFOROUSHAN, F., HATZFELD, D., ABBASI, M. R., VIGNY, C., MASSON, F., NANKALI, H., MARTINOD, J., ASHTIANI, A., BAYER, R., TAVAKOLI, F. & CHERY, J. 2004. Present-day crustal deformation and plate kinematics in the Middle East constrained by GPS measurement in Iran and northern Oman. *International Journal of Geophysics* **157**, 381–98.

VERNOOIJ, M. G. C., BROK, B. & KUNZE, K. 2006. Development of crystallographic preferred orientations by nucleation and growth of new grains in experimentally deformed quartz single crystals. *Tectonophysics* **427**, 35–53.

WAGNER, T., LEE, J., HACKER, B. R. & SEWARD, G. 2010. Kinematics and vorticity in Kangmar Dome, southern Tibet: testing mid-crustal channel-flow models for the Himalaya. *Tectonics* **29**, 1–26.

WALLIS, S. R. 1992. Vorticity analysis in a metachert from the Sanbagawa Belt, SW Japan. *Journal of Structural Geology* **14**, 271–80.

WALLIS, S. R. 1995. Vorticity analysis and recognition of ductile extension in the Sanbagawa belt, SW Japan. *Journal of Structural Geology* **17**, 1077–93.

WALLIS, S. R., PLATT, J. P. & KNOTT, S. D. 1993. Recognition of syn-convergence extension in accretionary wedges with examples from the Calabrian Arc and the Eastern Alps. *American Journal of Science* **293**, 463–95.

WANG, Y., ZHANG, Y., FAN, W. & PENG, T. 2005. Structural signatures and $^{40}Ar/^{39}Ar$ geochronology of the Indosinian Xuefengshan tectonic belt, South China Block. *Journal of Structural Geology* **27**, 985–98.

WELLS, M. L. 2001. Rheological control on the initial geometry of the Raft River detachment fault and shear zone, western United States. *Tectonics* **20**, 435–57.

XYPOLIAS, P. 2009. Some new aspects of kinematic vorticity analysis in naturally deformed quartzites. *Journal of Structural Geology* **31**, 3–10.

XYPOLIAS, P. 2010. Vorticity analysis in shear zones: a review of methods and applications. *Journal of Structural Geology* **32**, 2072–92.

XYPOLIAS, P. & DOUTSOS, T. 2000. Kinematics of rock flow in a crustal-scale shear zone: implication for the orogenic evolution of the southwestern Hellenides. *Geological Magazine* **137**, 81–96.

XYPOLIAS, P., CHATZARAS, V. & KOUKOUVELAS, I. K. 2007. Strain gradients in zones of ductile thrusting: insights from the External Hellenides. *Journal of Structural Geology* **29**, 1522–37.

XYPOLIAS, P. & KOKKALAS, S. 2006. Heterogeneous ductile deformation along a mid-crustal extruding shear zone: an example from the External Hellenides (Greece). In *Channel Flow, Ductile Extrusion and Exhumation in Continental Collision Zones* (eds R. D. Law, M. P. Searle & L. Godin), pp. 497–516. Geological Society of London, Special Publications no. 268.

XYPOLIAS, P. & KOUKOUVELAS, I. K. 2001. Kinematic vorticity and strain patterns associated with ductile extrusion in the Chelmos shear zone (External Hellenides, Greece). *Tectonophysics* **338**, 59–77.

XYPOLIAS, P., SPANOS, D., CHATZARAS, V., KOKKALAS, S. & KOUKOUVELAS, I. 2010. Vorticity of flow in ductile thrust zones: examples from the Attico–Cycladic Massif (Internal Hellenides, Greece). In *Continental Tectonics and Mountain Building* (eds R. D. Law, R. Butler, B. Holdsworth, M. Krabbendam & R. Strachan), pp. 687–714. Geological Society of London, Special Publication no. 335.

https://doi.org/10.1017/S0016756815000941 Published online by Cambridge University Press